Hall Basin and the Petermann Glacier, NW Greenland: A late Quaternary Provenance Glacial History

BLYTHE BEFUS

Department of Geological Sciences Honors Thesis

University of Colorado, Boulder

Thesis Advisor

Gifford Miller—Department of Geological Sciences, INSTAAR

Honors Council Representative

Charles Stern— Department of Geological Sciences

Committee Members

John Andrews— Professor Emeritus, Department of Geological Sciences & INSTAAR

Benjamin Teitelbaum—Assistant Professor of Ethnomusicology, Director of Arctic Studies

Anne Jennings—INSTAAR

APRIL 7, 2017

TABLE OF CONTENTS

ABSTRACT……... 3

INTRODUCTION……...4

BACKGROUND

GEOGRAPHIC SETTING……... 4

GEOLOGIC SETTING……. 7

MATERIALS……10

METHODS

MASS MAGNETIC SUSCEPTIBILTY……..10

XRD……..11

PARTICLE SIZE……..16

RESULTS

LITHOFACIES…….17

STATISTICAL ANALYSIS……...……..20

GRAIN SIZE RESULTS……...26

MINERALOGY, GRAIN SIZE, AND MASS MAGNETIC SUSCEPTIBILTY AT

DEPTH……..31

DISCUSSION……...36

CONCLUSIONS……...37

ACKNOWLEDGEMENTS……..39

REFERENCES……..40

APPENDIX……....42

ABSTRACT

The Petermann Ice Tongue, located in the northwest region of Greenland, has experienced large caving events since 2010. It is one of the few remaining ice tongues and or ice shelves still present in Greenland. The Petermann Glacier and its ice tongue are important to study as little is known about their glacial history since the deglaciation that likely began in the early Holocene. Through analyzing two cores, 18GC in Hall Basin and 003TC/41GC/003PC in the Petermann Fjord, in conjunction with prior analysis of the HLY03-05GC core in Hall Basin (Jennings et al., 2011), a relative glacial history of the Petermann Glacier is proposed. The mineralogy, grain size, and mass magnetic susceptibility were analyzed at 10-centimeter increments within the cores. A distinct lithofacies of laminated clays with almost no ice rafted debris (IRD) was observed in both the cores, as well in the HLY03-05GC core previously studied (Jennings et al., 2011). Based on knowledge of modern sub ice shelf sediments this laminated clay unit is tentatively interpreted to represent a sub ice shelf environment. The laminated clay unit is seen at the base of 18GC, overlain by a bioturbated mud unit. This transition from the laminated clay to bioturbated mud within 18GC is proposed to be representative of opening of Nares Strait around 9200 cal years BP. Within the composite core, 003TC/41GC/003PC, a shift from coarser grained sediment to the laminated clay unit is proposed to reflect the advance of the ice tongue site in the Petermann Fjord. This history of the Petermann Glacier contributes to the ongoing research being conducted in order to further understand the processes at work since the onset of the retreat of the Greenland Ice Sheet.

INTRODUCTION

The past history of the Greenland Ice Sheet (GIS) is important for gaining an understanding of how the ice sheet will respond to modern warming. The GIS is retreating today and contributing modern sea level rise. Ice shelves are important buttresses to ice sheets but the GIS only has a few remaining ice tongues in its northernmost part. One of these is the Petermann ice tongue that fronts the Petermann Glacier in Petermann Fjord (*Figure 1*). It is known that the Petermann Glacier was much bigger during the last glaciation than it is now (England, 1999), but there is little known about the history of the Petermann Glacier and its ice tongue during and since the deglaciation. This project uses new sediment cores from Hall Basin and the Petermann Fjord to understand how the Petermann Glacier and its ice shelf evolved during this time.

The objective of this thesis is to devise a late Quaternary glacial history of the Petermann Glacier and the Petermann Ice Tongue by examining relationships between mineralogy, grain size, and mass magnetic susceptibility for a suite of surface samples, samples from core catchers, and samples from two sediment cores, OD1507-18GC from Hall Basin, and composite core OD1507-3TC/3PC/41GC, from outer Petermann Fjord.

BACKGROUND

Geographic Setting

The Petermann Glacier is a 530-kilometer long, major outlet glacier of the Greenland Ice Sheet that forms an ice tongue in the Petermann Fjord on the northwestern Greenland margin. This ice tongue historically was about 80 to 90 km long and extended to the fjord entrance. It has undergone major calving events since 2010 that have shortened its length considerably and have

exposed seafloor that represents the sub ice shelf environment (Nick et al., 2012). The Petermann Fjord is over 1100 m deep in its central deep basin and it empties over a 400 m deep sill into Hall Basin at the northern end of the 500-kilometer long Nares Strait near the entrance to the Arctic Ocean (*Figure 1*; Tinto et al., 2015). Hall Basin is approximately 500 meters deep.

During the last glaciation, the Petermann Glacier was grounded throughout the fjord and extended into Hall Basin where it was confluent with other ice outlets from the Greenland and Innuitian ice sheets that formed an ice stream that emptied into the Arctic Ocean (England, 1974, 1985, 1999; Dyke et al., 2002; Jennings et al., 2011; Münchow et al., 2016). These confluent ice sheets blocked Nares Strait and it was only after the ice retreated that the connection between the Arctic Ocean and Baffin Bay was established. This event has been dated to c. 9200 cal years BP (Jennings et al., 2011). These events were captured in a sediment core, HLY03-05GC which has a laminated clay that was interpreted to be distal glacial marine overlain by a bioturbated mud with ice berg rafted clasts (IRD) that was deposited after the opening of the strait (Jennings et al., 2011).

The sediments examined in this thesis were taken on cruise OD1507 of the Swedish icebreaker, *Oden*, July- September of 2015. The sample types that were analyzed for this thesis include multicores, gravity and piston cores. *Figure 1.* is the site map displaying the locations of all the cores taken on the cruise, with the cores of focus for this thesis denoted with red stars. Core 18GC is located at 81.62°N, -62.29°E on the Greenland side of Hall Basin, and the composite core 003TC/41GC/003PC is located at 81.93°N, -61.97°E within the outer part of Petermann Fjord. The longitudinal coordinates of each core taken on the *Oden* can be observed in Appendix A.

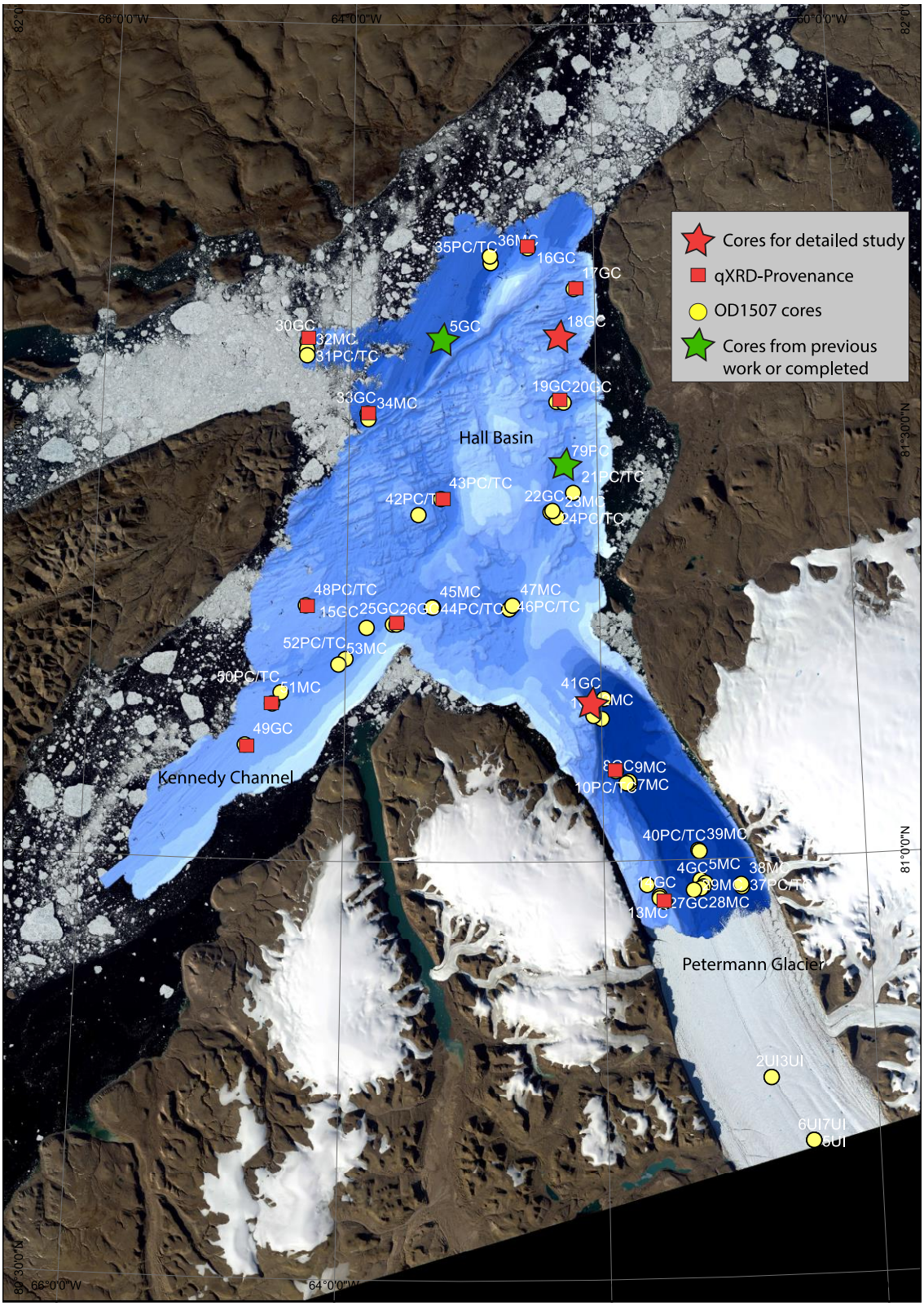

Figure 1.
Core site map of all cores collected on the Oden cruise OD1507
Cores in examination for this thesis are highlighted with red stars. Core 18GC is located at 81.62°N, -62.29°E. Composite core 3TC/41GC/3PC is located at 81.93°N, -61.97°E.
Map created using GPS coordinates taken on the expedition.

Geologic Setting

A knowledge of the geologic bed rock within Hall Basin, Petermann fjord, along the glacier and the various outlet areas surround the Petermann in Nares Strait is essential to tracking the provenance of the sediment examined within the cores. Provided in *Figure 2*. is the geologic map of Greenland (GUES, 2003). Extending into the fjord, along the present glacier edges is Lower Cambrian- Lower Silurian aged carbonate rocks. Cambrian and Silurian aged Carbonate rocks can also be found across the Kennedy Channel on the edge of Ellesmere Island. These carbonate rocks are composed of relatively soft minerals and therefore erode more readily into finer grain sized particles to be entrained in the current flowing through the strait. Near the terminus of the glacier and outer fjord walls are Silurian sandstones and silt stones. Glacial erosion of these larger grained sandstones and siltstones with a composition of more felsic minerals would be mineralogically and texturally distinct from the carbonate rock sources surrounding the glacier as well. Beneath the GIS are cratonic granitic gneissic rocks that have that would also have a felsic suite of minerals.

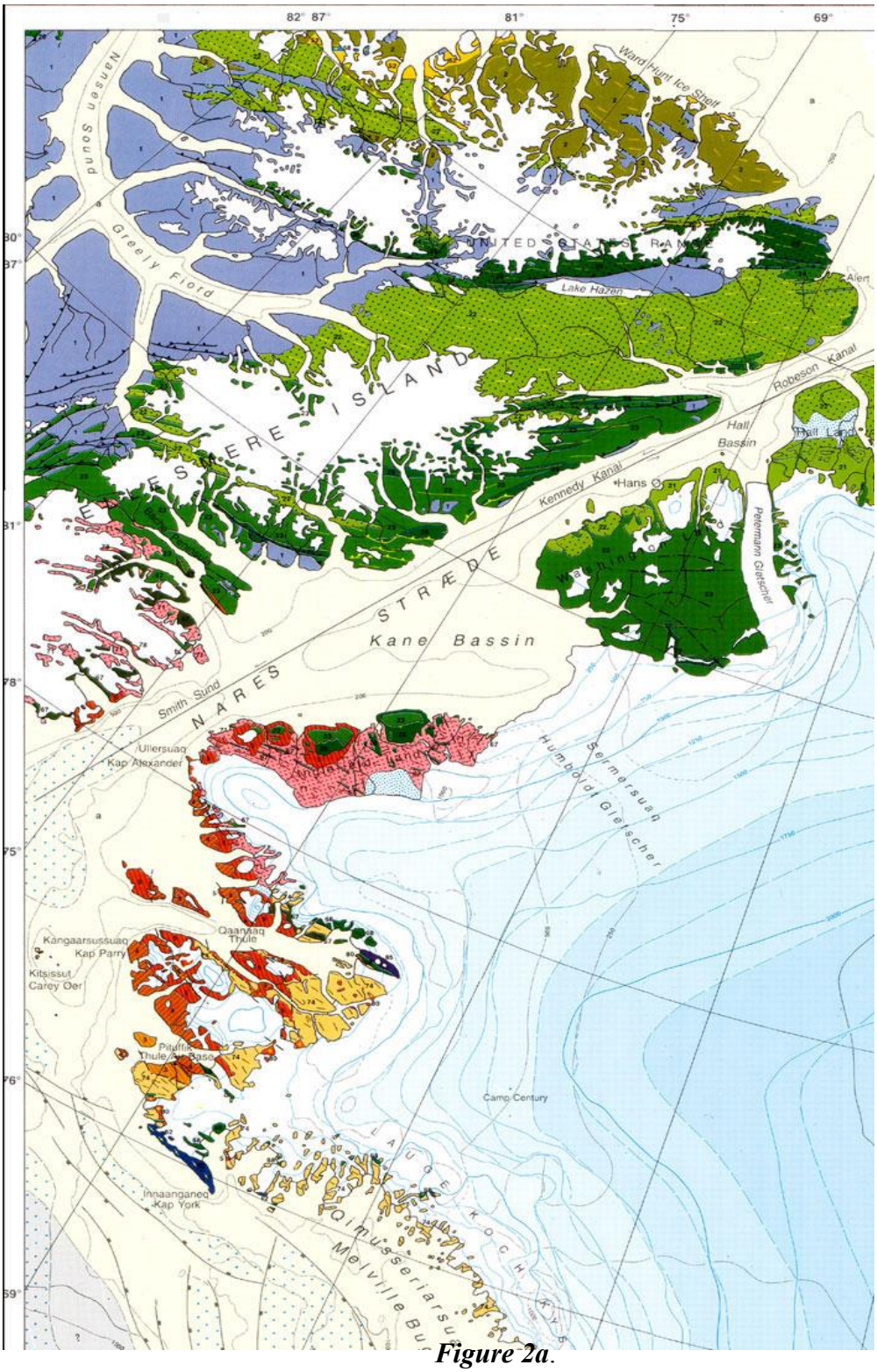

Figure 2a.
Geologic map of Greenland, section 5
Geologic Survey of Denmark and Greenland, 2003

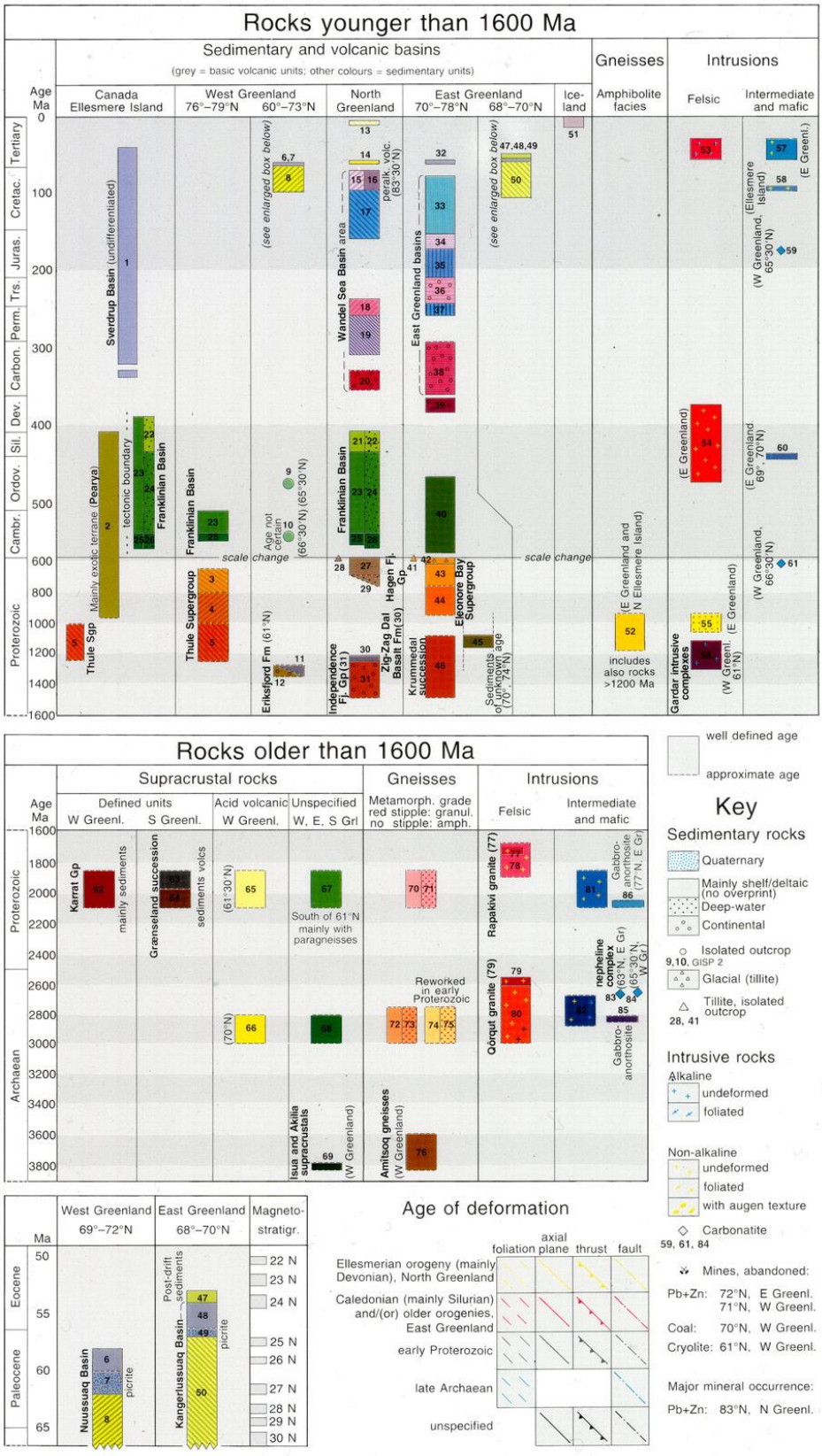

[1] Sverdrup Basin (undifferentiated). Unit occurs only on Ellesmere Island, Canada.

21] Silurian carbonates deposited on shelf and slope areas. Washington Land Group, Franklinian Basin, North Greenland.

[22] Silurian sand and siltstones deposited in deep water turbiditic trough. Peary Land Group, Franklinian Basin, North Greenland and Ellesmere Island.

[23] Lower Cambrian – Lower Silurian carbonates from shelf and slope areas. Brønlund Fjord, Tavsen Iskappe, Ryder Gletscher and Morris Bugt Groups. Franklinian Basin, North and North-West Greenland and Ellesmere Island.

Figure 2b.
Geologic map of Greenland key *Geologic Survey of Denmark and Greenland*, 2003

Materials

On board the *Oden* the OD1507, the expedition crew collected the cores and ran the whole round cores through the multi-sensor track (MST), split the cores, visually described them and photographed them using a digital line scan camera. The cores were shipped to Oregon State University (OSU) and CT-scanned at the veterinary hospital. The visual core descriptions, line-scan images and CT scans provide a down core visual of the physical characteristics and sedimentary structures present (*Figures 4a and 4b*). These resources allowed lithofacies that represent environmental changes to be defined (see Appendix B). Brendan Reilly, a PhD student at OSU, determined the overlap among 3TC, 3PC and 41GC, which were cores taken at the same site, using MST data and CT images. This information was used to develop a single composite core from the 3 cores that provides the most complete sediment record in the outer fjord. 18GC and the composite core were sampled for grain size and mineralogy at 10-cm intervals.

METHODS

Each core sample collected was run through a series of three procedures in order to analyze the magnetic susceptibility, particle size and mineralogy. All of the samples were weighed wet and then after drying in order to document the amount of sediment present, as well as to provide data to calculate equivalent dry weights of the foraminiferal samples.

Mass Magnetic Susceptibility

Once each sample was weighed dry, the magnetic susceptibility data was first collected. The magnetic susceptibility of a sample is a complex measure of both changes in mineralogy

(diamagnetic, paramagnetic and ferro magnetic minerals) and grain-size (Thompson et al., 1975; Walden et al., 1992). Ferromagnetic minerals, such as maghemite and other iron-titanium oxides, exert a greater magnetic susceptibility reading than diamagnetic minerals, such as quartz and calcite, which are negatively or weakly magnetic. Using lab prepped and labeled containers; each sample was distributed into their corresponding container and weighed to containing approximately 0.5 grams of sediment. Each weighed container was then inserted into a Bartington Magnetic Susceptibility Meter M.S.2. The raw output reading from the Bartington meter was the Total Susceptibility, * 10^{-5} SI. The total susceptibility and dry weight of each sample were then used to calculate the mass susceptibility, cubic meters per kilogram. The results are listed as * 10^{-7} m^3 /kg. Appendix C shows conversion of the total susceptibility to the mass susceptibility for a given example depth.

XRD

The samples were then prepared for testing of their mineralogies using the USGS protocol (Eberl, 2003). Each sample was first ground using a marble mortar and pestle, and sifted through a 2-millimeter sieve; any particles larger than 2 millimeters in diameter were put aside and weighed separately. Using the sieved sediment with <2 millimeter diameter, each sample was then weighed into 1 gram portion; bagging the remaining sediment into labeled storage bags. To each 1-gram portion of sediment, 0.111 grams (10% by weight) of zincite was added. Using 4 milliliters of ethyl alcohol, each sample was ground for 5 minutes in a McCrone Micronizing mill and air dried within a 35°C drier for at least 24 hours. Once dried, each sample was scraped from their labeled cup, ground in a mortar and pestle, and sieved once more before being packed into a labeled qXRD slide. The sample slides were then loaded and ran through the

Siemiens D5000 qXRD machine provided by INSTAAR, analyzing the sediment between the theta angles of 5 and 65 2-theta degrees. Once analyzed, the prepped zincite and sediment mixtures were placed in separate, labeled bags, only to be used again for further x-ray diffraction analysis.

Post collection analysis of the mineralogies was primarily preformed using the Excel program RockJock Version 6 (Eberl, 2003). The RockJock program takes the raw data and converts it to percent weight of the mineral constituents chosen to examine by the user. *Figure 3* shows the patterns configured in RockJock v.6, to which the program uses known peaks of standards of the minerals in question and compares them to the peaks measured in the samples to the best degree of fit (Eberl, 2003). The weight percentages in each sample were normalized and condensed into 15 mineral categories: quartz, potassium feldspar, sodium feldspar, plagioclase, calcite, dolomite, halite, amphibole, FeO minerals, SiO minerals, kaolinite, sphalerite, illite, muscovite, and biotite/chlorite. The categories, created for analyzing similar mineralogical components and minerals recurring throughout the cores formed simplicity and refined analysis. To check and maintain accuracy of both the Siemiens qXRD machine and the RockJock v.6 program, standards of known minerals and weight percentages were prepared and ran with each batch of core depth samples. One 3-gram standard mixture was made and separated into four XRD sample plates to be alternated through each run. Idealistically, all four of the standards would contain the same weight percentage of added sample minerals; however there will theoretically be variation between each standard sample and XRD run due to insufficient mixing, mineral orientation, etc. The RockJock v.6 program also provides the user with a full pattern degree of fit that can allow for examination of the accuracy (Eberl, 2003). Ideally the degree of fit would be zero, indicating that there is no discrepancy between the peaks of standard minerals

known by the program and the samples ran. If the degree of fit is <0.13, however, it is seem to be an acceptable representation of the minerals present. Any larger degrees of fit suggest that there are minerals missing from the analysis performed by the RockJock program. *Table 1* shows the normalized weight percentages of the minerals present in each standard ran, the average of each mineral's weight percentage, and standard deviation. There are two particular standards ran that are outliers, effecting the averages and standard deviation. The Standard 2 outlier specifically effected the quartz and plagioclase with significantly greater than the average weight percentages, while dolomite and FeO mineral weight percentages were significantly lower than the averages. Standard sample 3 also had an outlier run, affecting the same minerals however, in the opposite effect on the averages. The reason for the outliers is unknown and unexplainable. While these 2 outlier runs were measured, the rest of the standard samples ran remained consistent within their respective mineral weight percentages. The standard deviations of the standards run are displayed in *Table 1*, omitting the two outlying runs. While the standard errors are vastly different, nine out the eleven standard samples ran through the qXRD machine and RockJock analyses are consistent with each other's weight percentages and therefore assuming the data collected during this process to be reliable.

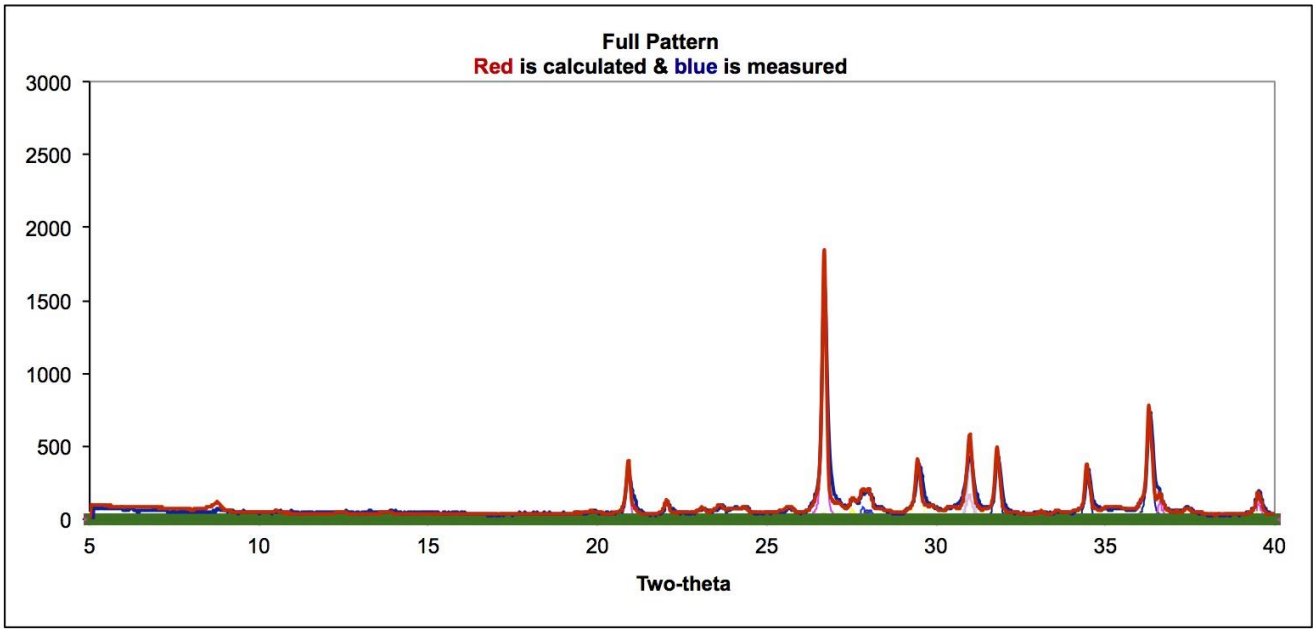

Figure 3. Graph generated for a randomly pulled sample of the cores displaying the full measured and calculated X-ray Diffraction pattern. Each mineral's structure corresponds to a unique intensity and two-theta angle. Close correspondence of the measured and calculated Ward's standard values seen implies reliability of the measurement.

	Degree of Fit	Quartz	Potassium Felds	Sodium Felds	Plagioclase	Calcite	Dolomite	Halite
STD 1	0.1	8.4	12.9	11.1	10.8	7.7	11.7	0.0
STD 1	0.4	6.7	9.5	5.8	2.0	6.4	2.2	1.8
STD 2	0.1	9.6	15.8	7.5	7.2	7.7	12.0	0.0
STD 2	0.1	8.7	11.9	9.7	11.5	7.1	12.5	0.0
STD 3	0.2	6.8	9.8	6.5	2.4	10.4	0.1	0.3
STD 3	0.2	5.8	10.2	7.9	1.9	9.5	0.2	0.0
STD 4	0.1	6.0	11.8	4.7	2.7	10.6	0.0	0.0
STD 4	0.1	6.6	11.3	4.1	3.0	10.2	0.0	0.0
STD 4	0.2	7.3	9.7	6.4	2.7	10.9	0.1	0.0
AVERAGE		7.3	11.4	7.1	4.9	8.9	4.3	0.2
STD. DEV.		1.29	2.03	2.25	3.87	1.72	5.86	0.59

	Amphibole	FeO Minerals	SiO Minerals	Kaolinite	Saphalerite	Illites	Muscovite	Biotite & Chlorite
STD 1	0.1	16.8	3.2	7.7	3.3	4.7	3.3	0.9
STD 1	0.7	20.2	18.5	10.0	13.6	9.3	0.0	11.2
STD 2	11.3	7.0	6.1	7.5	1.7	5.6	4.0	3.1
STD 2	0.0	15.9	1.8	7.6	2.4	4.5	3.5	4.6
STD 3	0.4	23.0	19.5	18.7	5.4	13.4	0.9	1.2
STD 3	0.0	24.1	20.5	19.4	2.0	11.3	0.0	6.5
STD 4	0.0	27.4	23.8	19.3	3.9	12.4	0.0	0.5
STD 4	0.0	24.7	21.2	18.7	2.8	12.6	0.0	5.3
STD 4	0.0	20.8	17.8	19.5	3.8	14.0	0.6	3.4
AVERAGE	1.4	20.0	14.7	14.3	4.3	9.8	1.4	4.1
STD. DEV.	3.72	6.13	8.50	5.80	3.65	3.86	1.70	3.37

Table 1.

Normalized weight percentages of minerals within each the standard mixture prepare and ran through each qXRD batch for accuracy control; standard mixture was prepped October 21, 2016 and used throughout the entirety of the XRD measurements. The table displays the standards ran, omitting the two deviatory runs with large errors.

Particle Size

The remaining sediment of each core sample was then prepped for particle size analysis using a Malvern Mastersizer 3000. One gram of each sample was measured out into separate, labeled 600-milliliter beakers. To each measured sample, approximately 5 milliliters of 30-35% hydrogen peroxide and distilled water were added before each being placed on a series hot plates to burn off the organic material within the core samples. Once the reaction of the removal process ceased, the beakers were taken off the hot plates and wet sieved through a series of three stacked sieves, 2 millimeter, 125 micrometers, and 850 micrometers, into another set of labeled beakers—to which 8 milliliters of magnesium chloride and 500 milliliters of distilled water was added to settle for 24 hours. Once the sediment had settled to the bottom, the distilled water was decanted from each beaker and the sediment transferred to labeled centrifuge tubes, centrifuged, and remaining liquid poured off. The sediment was then allowed to sit with 20 milliliters of sodium metaphosphate for 24 hours before being spilt three times and ran through the Malvern Mastersizer 3000.

The programs GRADISTAT (Blott and Pye, 2001) and KaleidaGraph (Synergy, 2014) were used to process and analyze the particle sizes obtained from the Mastersizer. The GRADISTAT program uses many numerical and descriptive methods of analyzing the particle sizes primarily from Folk and Ward (Blott and Pye, 2001) The KaleidaGraph program was used to plot the range of particle sizes per core to analyze any recurring patterns between the cores and at depth (Synergy, 2014). Examining the grain size distribution can help in analyzing shifts in the modes of transportation and sedimentation with time of the Petermann's evolution relative to the opening of the Strait with the retreat of the Greenland Ice Sheet. Typical glacial marine deposits transported by entrainment within the magnitude of approximately 0.1 to 50 microns,

silt sized sediment. Larger grained clasts of approximately 500-2000 microns are indicative of ice-berg rafting and are interpreted as ice rafted debris (IRD). In Hall Basin, the presence of abundant IRD sized clasts (*Figures 4a-b, 7a-c.*) indicates the opening of the Strait to allow icebergs to move away from the ice front and transport and deposit of the IRD clasts. In the Petermann Fjord, abundant IRD likely suggests deposition outside beyond the ice shelf front. Observations of the grain size distributions at depth are further discussed in the results section of this thesis.

RESULTS

Lithofacies

Observation of the CT scans and core descriptions (*Figure 4a, b, A*ppendix B) allowed me to define lithofacies for each core. Core 18GC has 2 lithofacies. The base of the core to 115 cm is laminated clay with sand layers and dispersed, rare IRD. From 115 cm to the core top is bioturbated mud with dispersed rare IRD that is more common than in the laminated clay. There is an interval of higher IRD between 320 and 300 cm. There is an interval of high IRD between 112 and 98 cm at the transition between the 2 lithofacies.

The composite core has 5 lithofacies. The base of the composite core has massive diamicton with large clasts (1-5 cm diameter) from 555 to 519 cm. From 519 to 489 cm is laminated clay with intermittent sand/clast layers with dispersed IRD. From 489 to 412 cm is vaguely laminated clay with rare IRD. From 412 to 342 cm is distinctly laminated clay. From 342 to 172 is homogeneous clay with dispersed IRD. From 172 to the core top is bioturbated clay with very rare dispersed IRD.

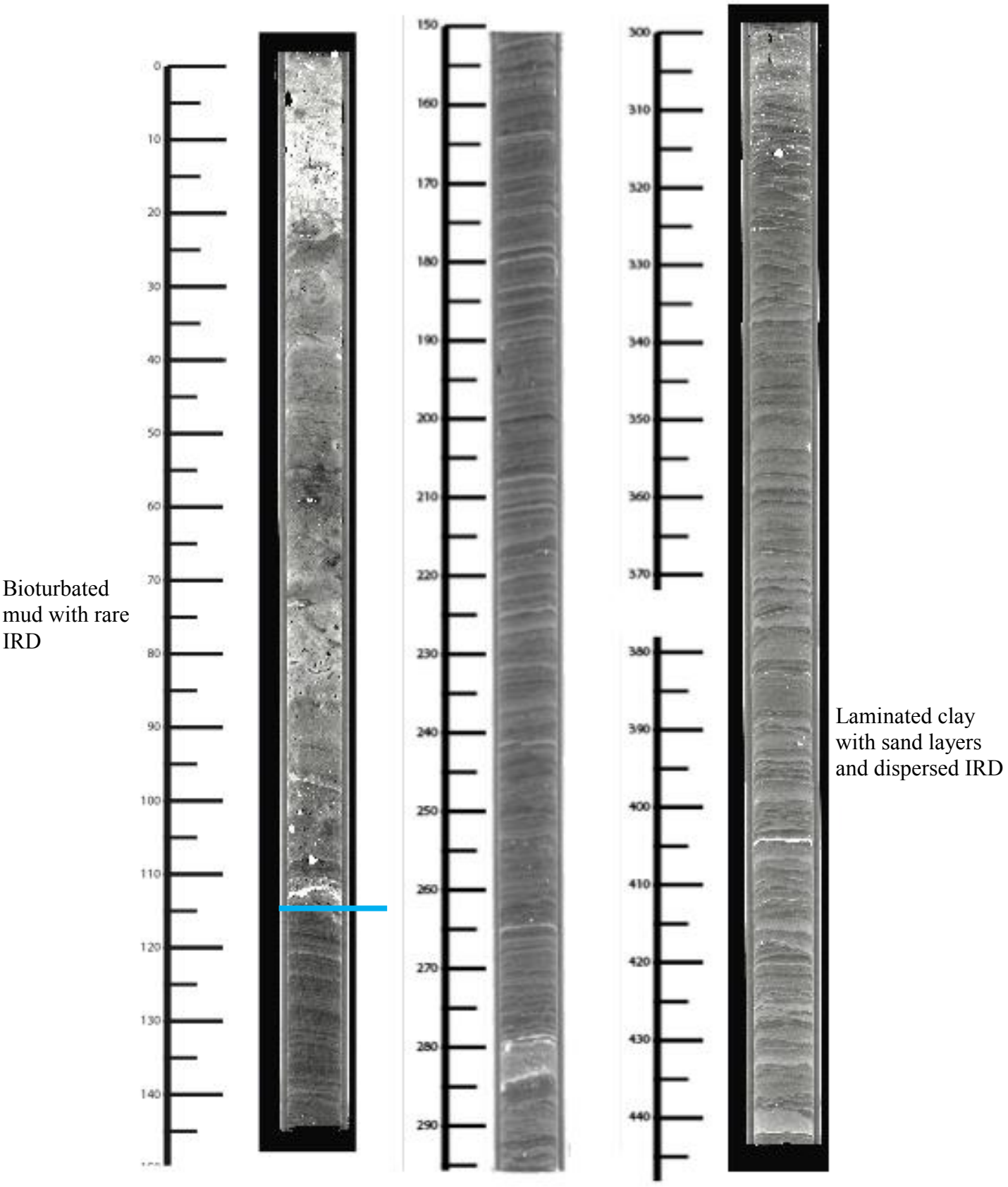

Figure 4a. CT scans taken of core 18GC

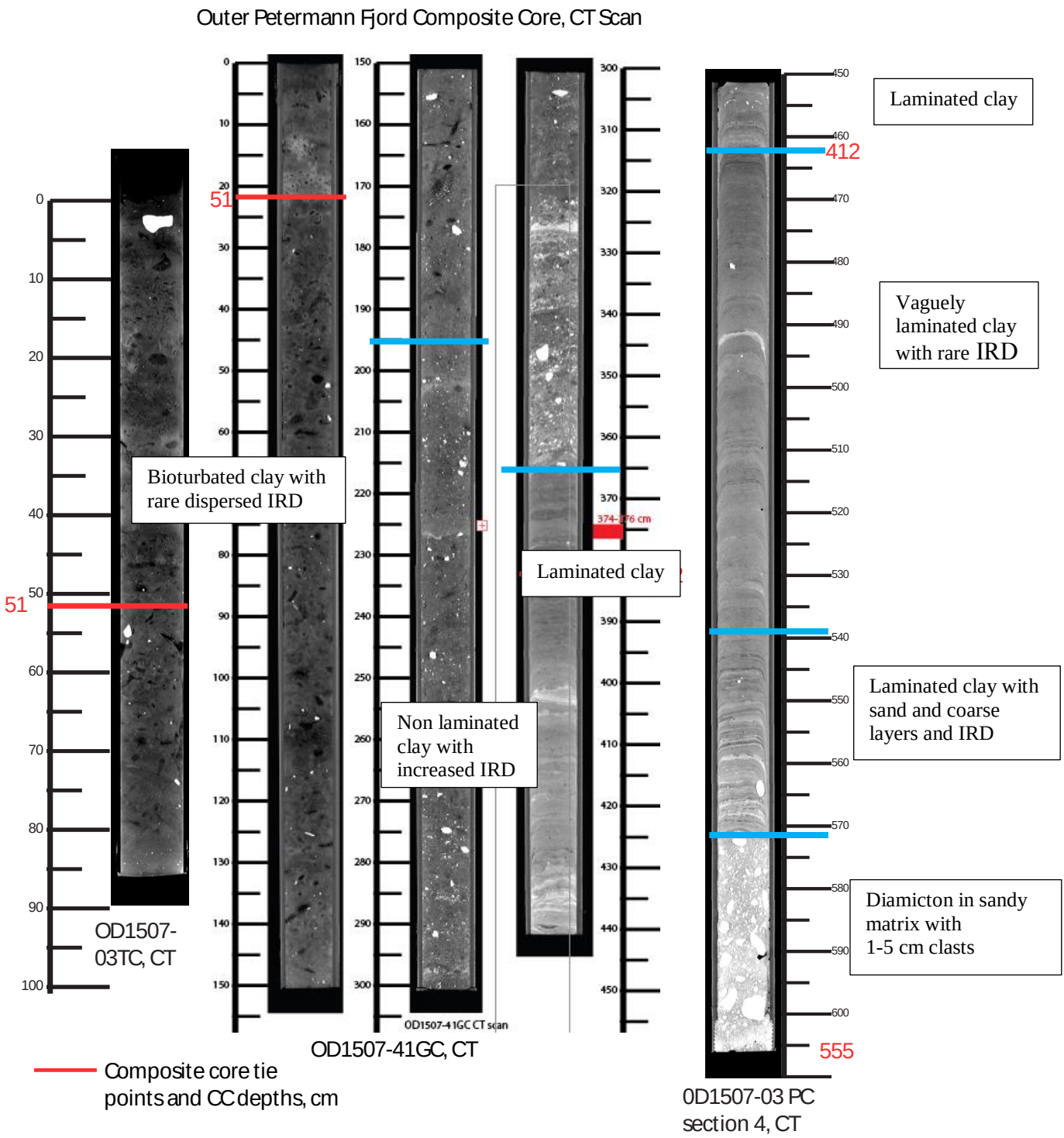

Figure 4b. CT scans of each respective core making up the composite core 3TC/41GC/3PC. Composite core depths were adjusted using Magnetic Susceptibility data by Brendan Reilly.

Statistical Analyses

All of the mass magnetic susceptibility, mineralogy, and particle size data from 18GC and 003TC/41GC/003PC were entered into the program Abel v.3 for statistical analysis. Within the Abel program, the statistical analysis method of k-mean clustering was employed (Gigawiz, 2008). The K-mean Clustering analysis takes the data set at hand and divides it iteratively into *k* number of similar groups. Through a series of iterations, the k-mean clustering selects a mean point within each of the arbitrarily assigned groups, adjusts points and group assignments to minimize the deviation of the points from the mean of their assigned group, and iterates this process until the optimal groups have been calculated. The user determines the number of groups, k, desired (Ghosh and Dubey, 2013). A total number of groups, k=4, was first analyzed. *Figure 5a* shows the resulting clusters. There is a clear outlying group, D, whose distinction is being influenced by a uniquely defining mineral or group of minerals that groups A-C do not contain. Between the two end member clusters, A and C, is a middle lying group, B, which seems to be within the overlap of A and C. With a middle, seemingly transitional group, not much mineralogical distinction can be made from it to either end members. Another k-mean clustering analysis was then ran through Abel with k=3 groupings to minimize the effects of this transitional group. *Figure 5b* shows the resulting groups with k=3. The outlying group, labeled G, is still present, but the transitional group had now been dispersed between the two end member groups, now labeled E and F, creating clear distinction between each cluster, each with a defining mineralogical component or assemblage influencing its distinction. It can be hypothesized that the groups are not only distinct in terms of a defining mineralogical component but by mean grain size as well. Dependence on quartz and other felsic minerals such as the various feldspars are more resistant to weathering than mafic minerals such as the biotites, and

would therefore influence dependence on a higher mean grain size. Dependence on carbonate minerals would also induce dependence on smaller grain size particles, as carbonate minerals are also more susceptive to weathering and erosion. I determined that the k=3 cluster was the better representation of the distinct mineralogical components.

Principal components analysis (PCA) of the mineralogical data in both of the cores shows two major PCA axes. Muscovite has high positive loadings on PCA Axis 1 and Na feldspar has the highest negative loadings on PCA Axis 1. Quartz and calcite have high positive loadings on PCA 2 whereas Fe-oxides and Silicates have high negative loadings on PCA 2.

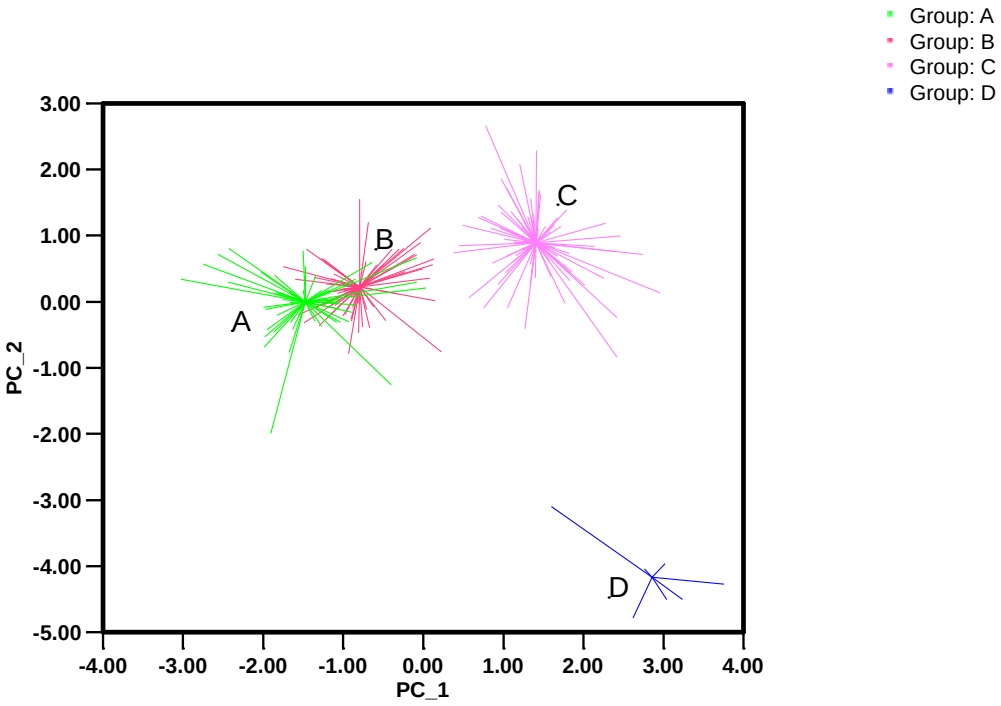

Figure 5a.
K-mean clustering, k=4, resulting clusters

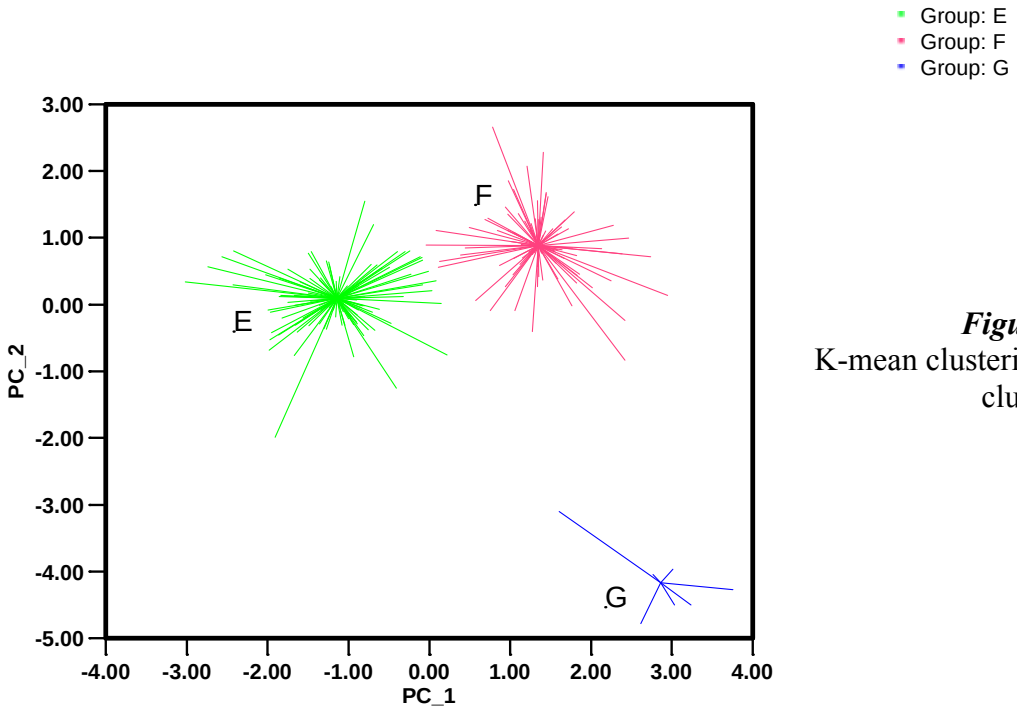

Figure 5b.
K-mean clustering, k=3, resulting clusters

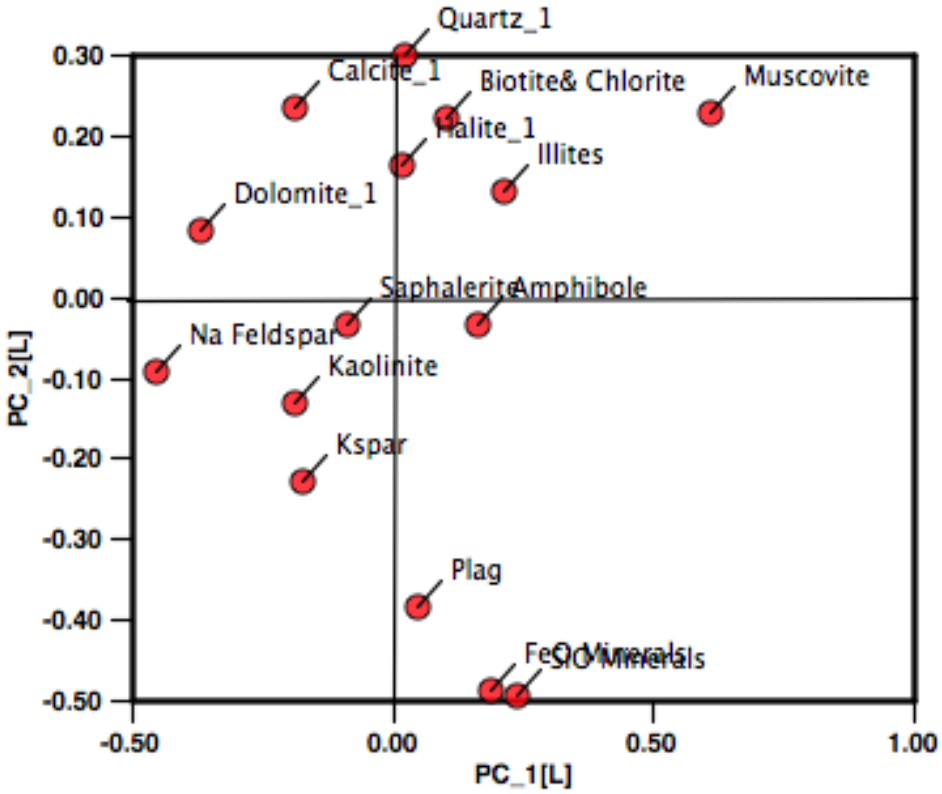

Figure 5c.
Principal components 1 and 2 plotted against each other to examine the most influential minerals to the data set. Principal components 1 and 2 were examined because they represent over half of the data present. Quartz, calcite, FeO minerals, and SiO minerals are most influential to principal component 2. Muscovite, sodium feldspar, and dolomite are the most influential mineral to principal component 1.

Core catcher (samples from the bottoms of the cores) and surface samples (multicore tops) collected from the same sites provide a comparison of long-term changes in sediment provenance and sedimentation processes in the study area. The difference in percent constituents of mineralogies and mean grain size (microns) were calculated and surface sample values subtracted from the core catcher values to give trends with time approaching present. The difference in quartz abundance from core catcher to surface was first examined. Use of Ocean Data Viewer's (ODV; Schlitzer, 2016) gridded field function gives an interpretation of the quartz abundances across Nares Strait and the Petermann fjord shown in *Figure 6a*. Based on the paired comparison (not on the composite core), quartz increases with time within the fjord (*Figure 6a*). Based on quartz's mineralogical property of resistance to physical weathering and from the observation of increasing quartz within the fjord, I hypothesized that the mean grain size also would increase with time to present in the fjord as well. Further, an increase in the mean grain size within the fjord could indicate either a decrease in abundance of softer minerals such as carbonates, feldspars, or micas or a decrease in the transport of sediments in suspension associated with suspended melt water plumes, or retreat from a sub-ice tongue environment, which is in general fine grained. To test these hypotheses, the difference values of biotite, calcite, dolomite, and mean grain size were plotted. As hypothesized, there was a decrease of both carbonate minerals examined within the fjord with time through present (*Figure 6c and 6d)*. There is also a notable trend of decreasing biotite and chlorite abundance from the northern edge of the Petermann Fjord across the Nares Strait, increasing within the fjord itself. However, examining *Figure 6f*, the mean grain size within the fjord with time has decreased. One explanation for this could be that the opening of the Nares Strait with glacial retreat, allowed for a current to flow through the Strait carrying sea ice and icebergs with it and winnowing the

sediments, leading to coarser grain sizes in Hall Basin. But in the Petermann Fjord the mean grain size decreased which might be related to formation of the ice tongue.

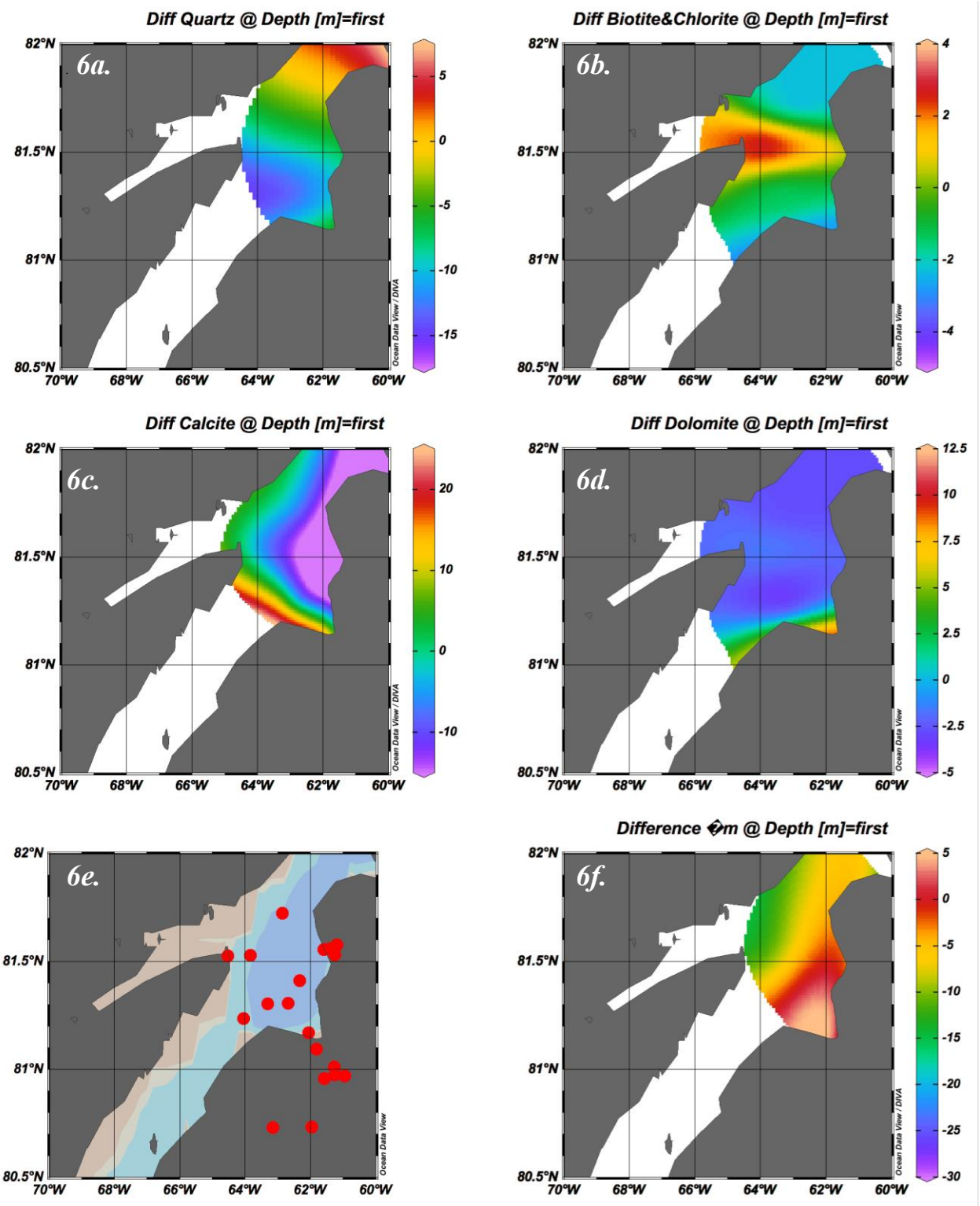

Figure 6.
Differences of mineral constituents and mean grain size (microns) calculated from subtracting the surface sample data from the core catcher data collected of cores across Hall Basin and Petermann Fjord.
Note: A negative value in the figure corresponds to an increase over time to present. A positive value in the figure corresponds to a decrease over time to present.

Grain Size Results

Overall, the grain size distributions of both 18GC and 003TC/41GC/003PC are poorly to very poorly sorted sediment with mean grain size of very coarse to fine silt-sized grains. The distribution plots (*Figure 7a-c.*) display distinct bi-, tri, and polymodal (>3 modes) distributions, which are in keeping with the alternating laminations and the varying dispersed IRD components as determined from the CT scans of *Figures 3a-b*. The different grain-size modes suggest that there were three sediment transport processes at work in the area.

The distribution of the grain sizes for core 18GC ranged from approximately 0.405 to 2000 microns, with an average grain size of 6.15 microns (i.e. fine silt). The distribution of grain sizes displays tri- to polymodal distribution (*Figure 7a*). The grain size modes encompassing <1-micron and 4-20 micron grains are interpreted to be represent of glacial marine sediment transported and entrained in freshwater issuing from the glacier grounding line. Figure 7a shows that these modes are highest in the laminated clay and the transitional unit. . Between these two distinct modes is a low abundance of approximately 2-micron sized grains. This anomalous dip in the distribution of grain sizes is not unique to the 18GC core, as it was observed in all grain size distributions, for all for all of the cores examined in the project. This systematically occurring anomaly was also observed by a grain size analysis performed by Anna Klein of sediment from Baffin Bay, in which the same Malvern machine was used (Klein, 2016). It has hence been interpreted as being an instrumental error and the instrument manufacturer is being contacted to evaluate this issue (Wendy Roth, person in communication, 2017). Referring back to *Figure 7a.*, there is also a third distinct mode at grain sizes >100 microns. This mode is interpreted to represent the thin sand layers and rare coarse IRD.

The distribution of grain sizes within 003TC/41GC/003PC core ranged from approximately 0.3 to 2000 micron sized grains, with an average grain size of 9.34 microns—coarser than that of 18GC. The distributions of grain sizes within the composite core have tri-modal distributions, indicative of three modes of sediment transport (*Figure 7c*). Similar to 18GC, two modes ranging from approximately 0.3 to 1 micron and 3 to 100 microns are observed, also proving to display the assumed instrumental error induced anomaly at approximately 2-microns. The approximate >100-micron ice rafted sediment mode is also evident, but is to be noted to only be present at deeper depths within the core and to decrease in abundance toward the surface (*Figures 3a and 7c*). There is a fourth distinct mode observed in the composite core at depth, occurring within the sandy region of the distribution plot, approximately 90 to 700 microns in size. Samples with the high abundance of sand grains occur within the depth range of 524.6 to 554.6 meters, in the diamicton at the base of 003PC section of the composite core. In these grain size spectra, the spike in abundance of sand grains coincides with a relative decrease in abundance of the silt and clay sized grains. These grains are far too large to have been transported through entrainment, while also being smaller than average ice rafted debris sediment. However, observed coarse clasts, up to 5 cm in the diamicton, are not measured in the grain size analysis, which is limited to <2 mm materials. The sediment could have been transported in a number of ways, including but not limited to debris flow deposition, turbid eddy deposition, or sub glacial fluvial deposition with the retreat of the ice sheet and glacier. While the exact transport mechanism and source of this sediment is unknown, it is an interesting break in the pattern of transport seen within the area that could be further investigated. The grain size spectra in 3TC are very similar to one another and have only 2

modes once again separated by the anomaly. These spectra indicate very consistent sedimentation processes likely representing the environment beneath the ice tongue.

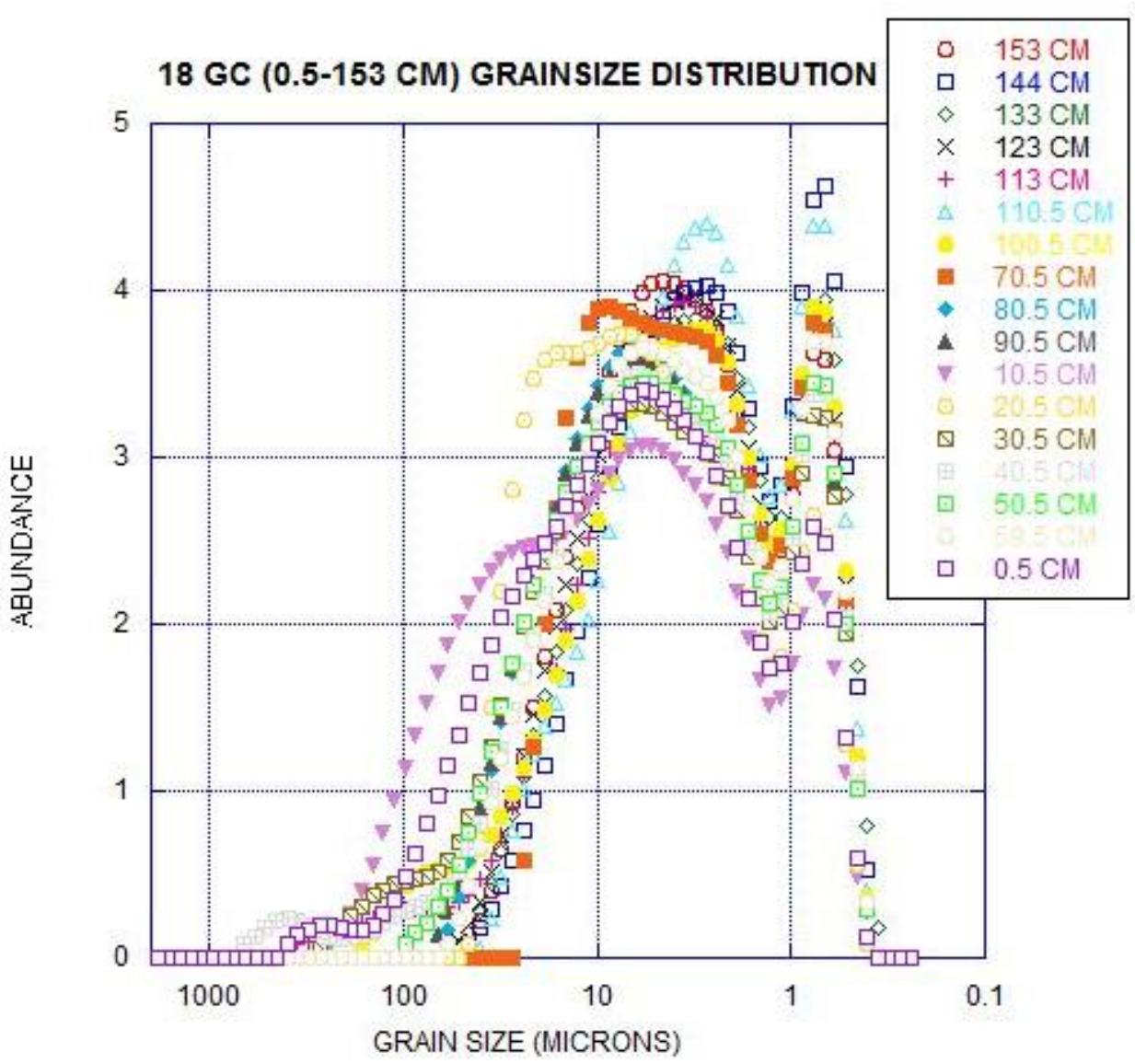

Figure 7a.
Grain size distributions of top 153 centimeters of the 18GC core created on KaleidaGraph. Bi- and tri-modal patterns arise at depth. Both lithofacies are represented.

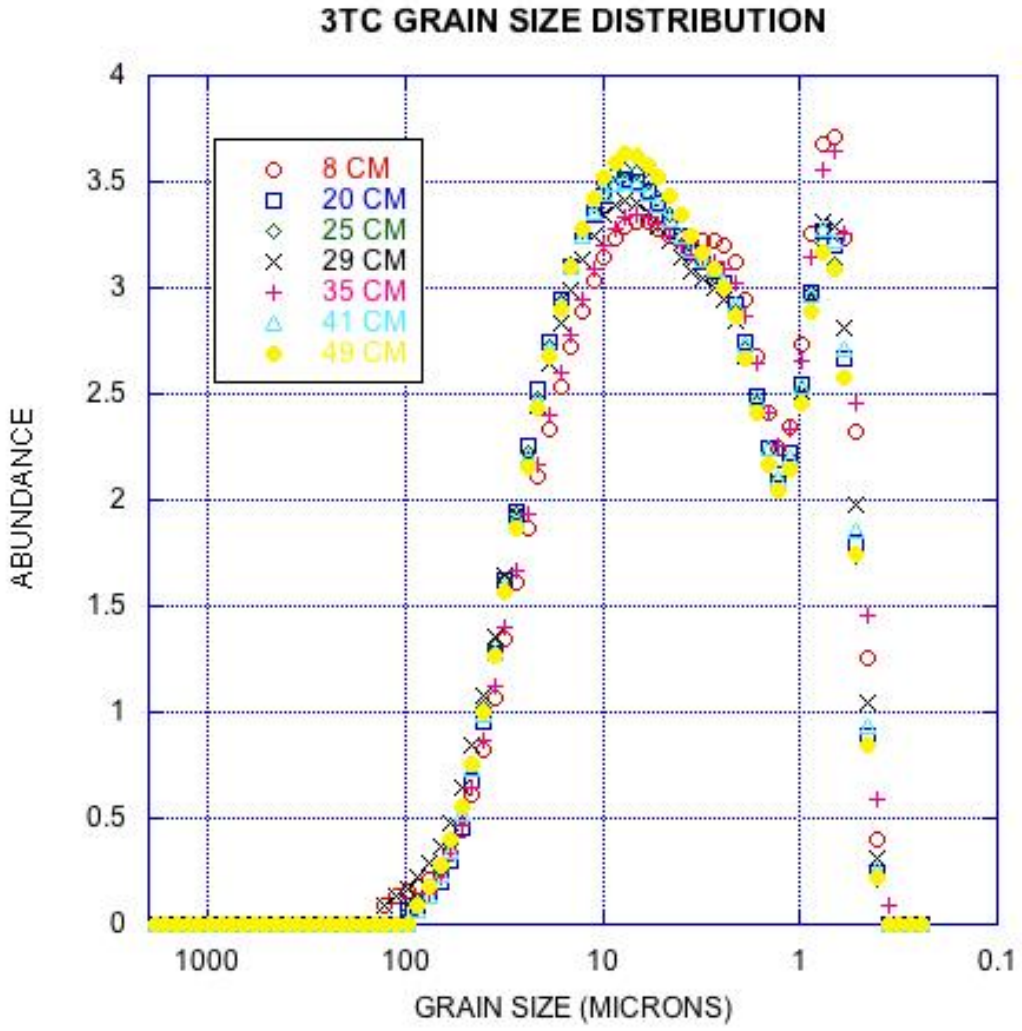

Figure 7b.
Grain size distribution of 003TC of the composite core 003TC/41GC/003PC created on KaleidaGraph. This section of the composite core displays a bimodal distribution in grain size.

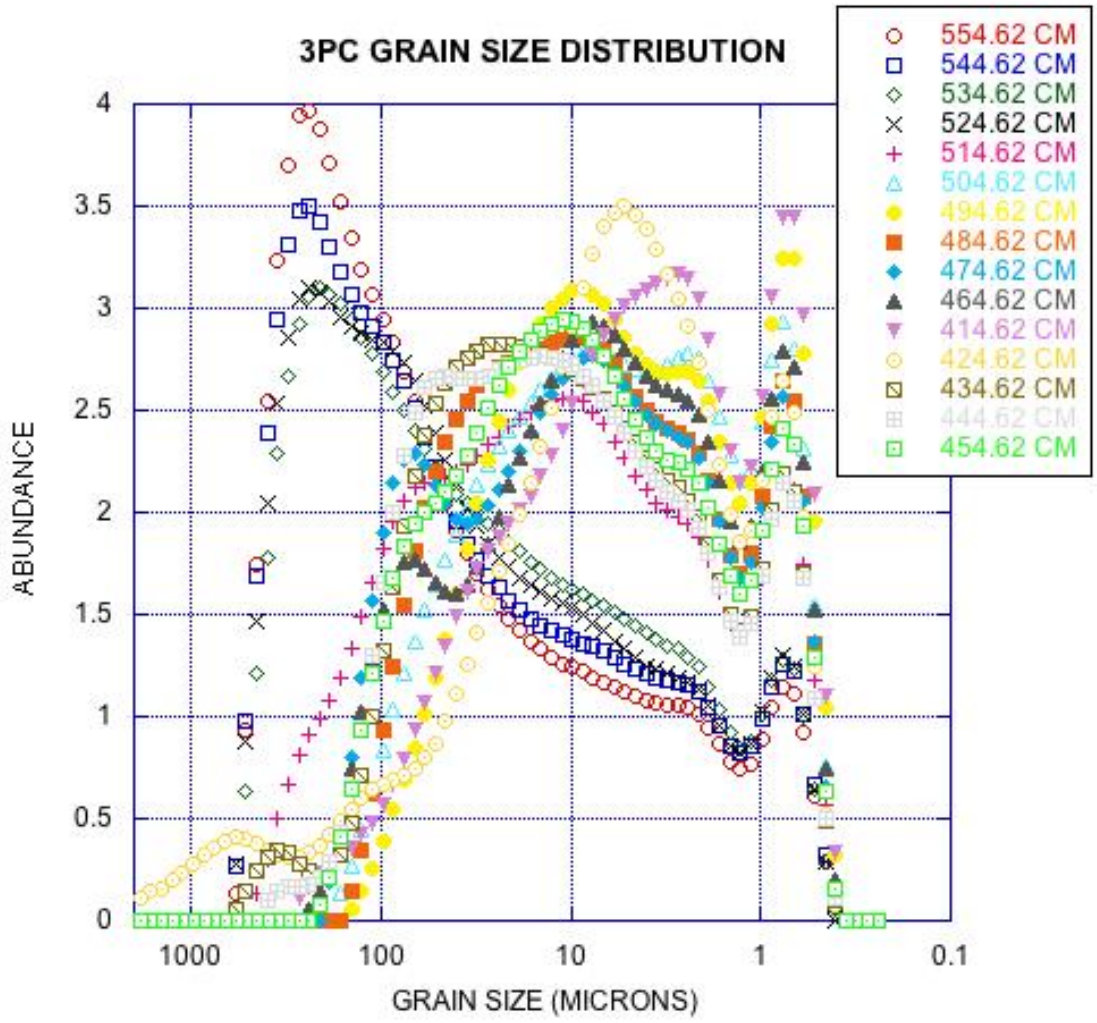

Figure 7c.
Grain size distribution of 003PC of the composite core 003TC/41GC/003PC created on KaleidaGraph. This section of the composite core displays bi-, tri, and polymodal distributions in grain size.

Mineralogy, Grain Size, and Mass Magnetic Susceptibility at Depth

Detailed down core analysis of both 18GC and 003TC/41GC/003PC cores were compiled into *Figures 8a and 8b*, to compare the weight percent of the major mineralogical components, mean grain size, grain size descriptors, and mass susceptibility against the lithofacies.

Mineralogical differences are more evident within the composite 003TC/41GC/003PC core than within 18GC, possibly reflecting the more complex depositional history in the fjord. The weight percentage of quartz varies greatly in the fjord core. The maximum weight percentage of quartz is 25% and first occurs in the diamicton at the base of the composite core at a depth of 515-555 centimeters. Present also at this depth is the coarser mean grain size of 70 microns and maximum magnetic susceptibly of ~$15*10^{-6}$ m^3 /kg. The lowest weight percentage of quartz within the composite core occurs at the interval of 465-404 cm, the laminated clay with IRD facies. Within this interval of low quartz concentration, there is an interesting variation in the other minerals weight percentages. With the sudden decrease in quartz presence, there is also a rapid decrease in the carbonate and sodium-rich feldspar weight percentages. This is expressed as an increase in plagioclase, muscovite and potassium feldspar, with the maximum plagioclase and muscovite percentages of 40 and 35% respectively, occurring approximately simultaneously at the depth of no quartz being present. However, I note that an important issue with the use of percentage data is that, by definition if one mineral decreases in percentage then by definition, one or more other minerals have to increase (Aitchison, 1992, 1997, 1999; Davis, 1973). The sediment directly overlying this quartz low, rebounds within around 50 centimeters of sediment to a second and third maximum quartz weight percentage around 25%, with a parallel increase in the mean grain size and magnetic susceptibility as well. This interval is contained within the lithofacies of vaguely laminated clay with rare IRD. Within this lithofacies, carbonate minerals

decrease in abundance. Following these maxima of quartz is another rapid decline of quartz concentration to weight percentages as low as 5% at 344 centimeters depth. Unlike the previously observed minimum, there is a slight increase in the carbonate minerals and no change in the plagioclase, potassium feldspar, or muscovite weight percentages. It is at this depth of approximately 344 centimeters that the dramatic sediment fluctuations cease to occur as the weight percentages, mean grain size, and magnetic susceptibility level off to mean values to the near surface.

A similar analysis of the mineralogical variations with depth was preformed along the length of 18GC. The mean grain size of the base of 18GC is quite fine, near the calculated average of 6.15 microns. This is quite similar to the upper 344 cm of the fjord core. The weight percentage of quartz does not vary as dramatically as within the composite core; this is relatively true for all of the minerals in focus of 18GC. Overall there is little fluctuation in the parameters in 18GC, reflecting a stable environment. Around the base depth of 433 centimeters is a spike of weight percentage muscovite to approximately 15-20%. In the fjord core there is one interval of high muscovite at 433 centimeters suggesting the source for this muscovite may lie within the fjord bedrock. At a depth of approximately 295 centimeters, there is a decrease in the total dolomite and plagioclase weight percentages and a spike in the mass magnetic susceptibility. Because neither the mean grain size nor the ferromagnetic mineral weight percentages, including Fe bearing dolomite varies at this depth, the source of the increased magnetic susceptibility is unknown. There are two relative minima of quartz weight percentages within 18GC, one occurring at approximately 193 centimeters depth and the other at 163 centimeters depth. As previously observed in this core, the other mineral constituents do not vary relative from their mean at these intervals. A noticeable ever-increasing mean grain size trend can be observed by

looking at the entirety of 18GC. The mean grain size increases in the upper lithofacies reach a maximum of approximately 8 microns at 10 centimeters depth, relatively near the surface. However, the scale of the mean grain size plots differs dramatically between the two cores (*Figure 8)*. This is an important observation to make, as the maximum mean grain size within 18GC of 8 microns is only approximately a 5-micron increase from the minimum mean grain size of 3 microns. Descriptively this is a variation from very fine silt to fine silt, a small relative change in the grain size that does not imply a dramatic shift of transport or events, even though the lithofacies shift is visually dramatic. Comparatively, the maximum mean grain size within the composite core is approximately 65 microns larger than the minimum and average mean grain size of 5-6 microns. But, the composite core converges in mean grain size with 18GC in the upper unit. This is further discussed and expanded on below in the discussions section of this thesis.

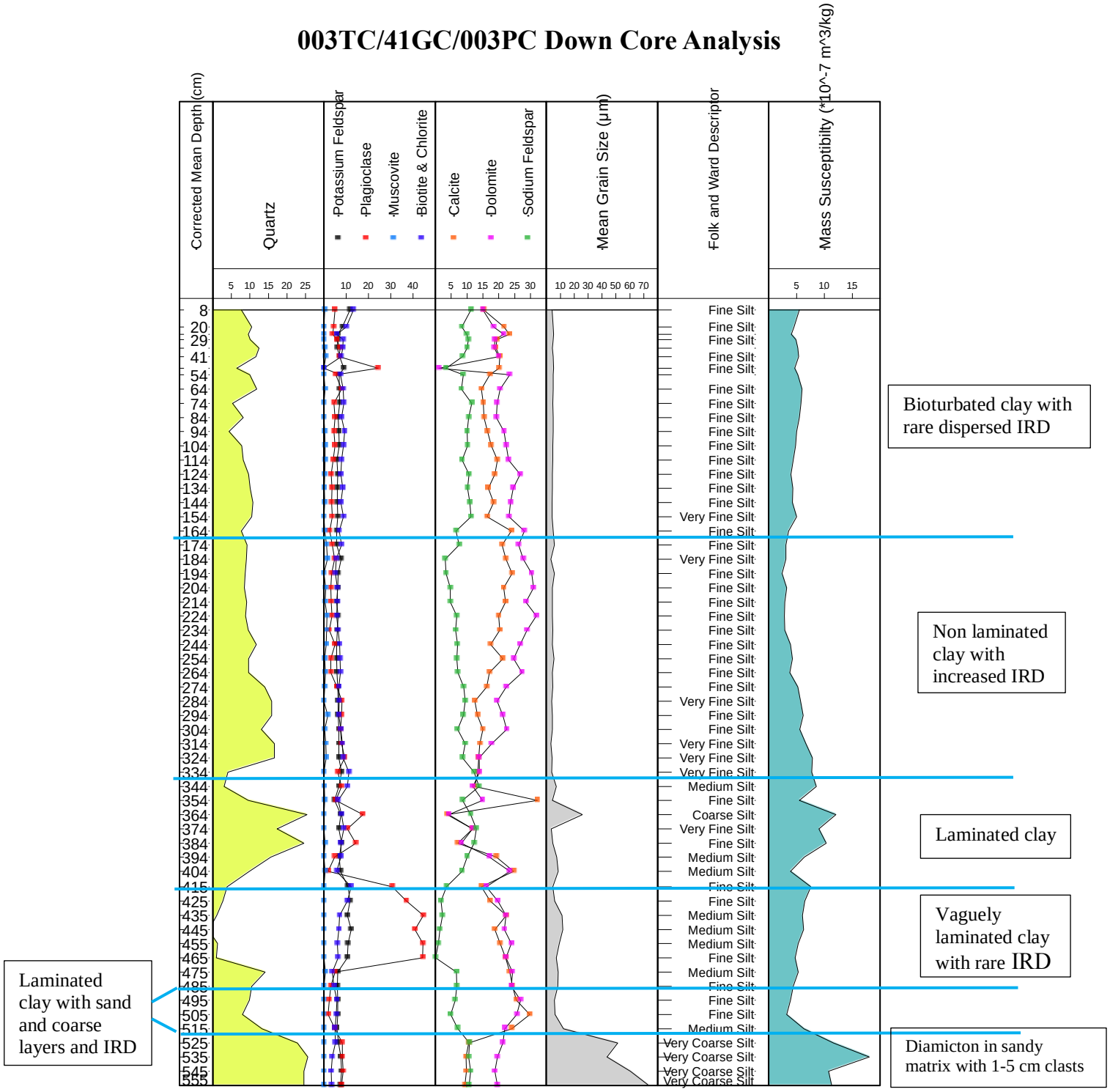

Figure 8a. Down core plot of 3TC/41GC/3PC graphically showing the measurements (taken using procedures in the Methods section of the theses) with depth. Weight percentages were accumulated from the RockJock v6 program (Eberl, 2003). Folk and Ward descriptors and mean grain size calculated by the GradiStat program (Blott and Pye, 2001)

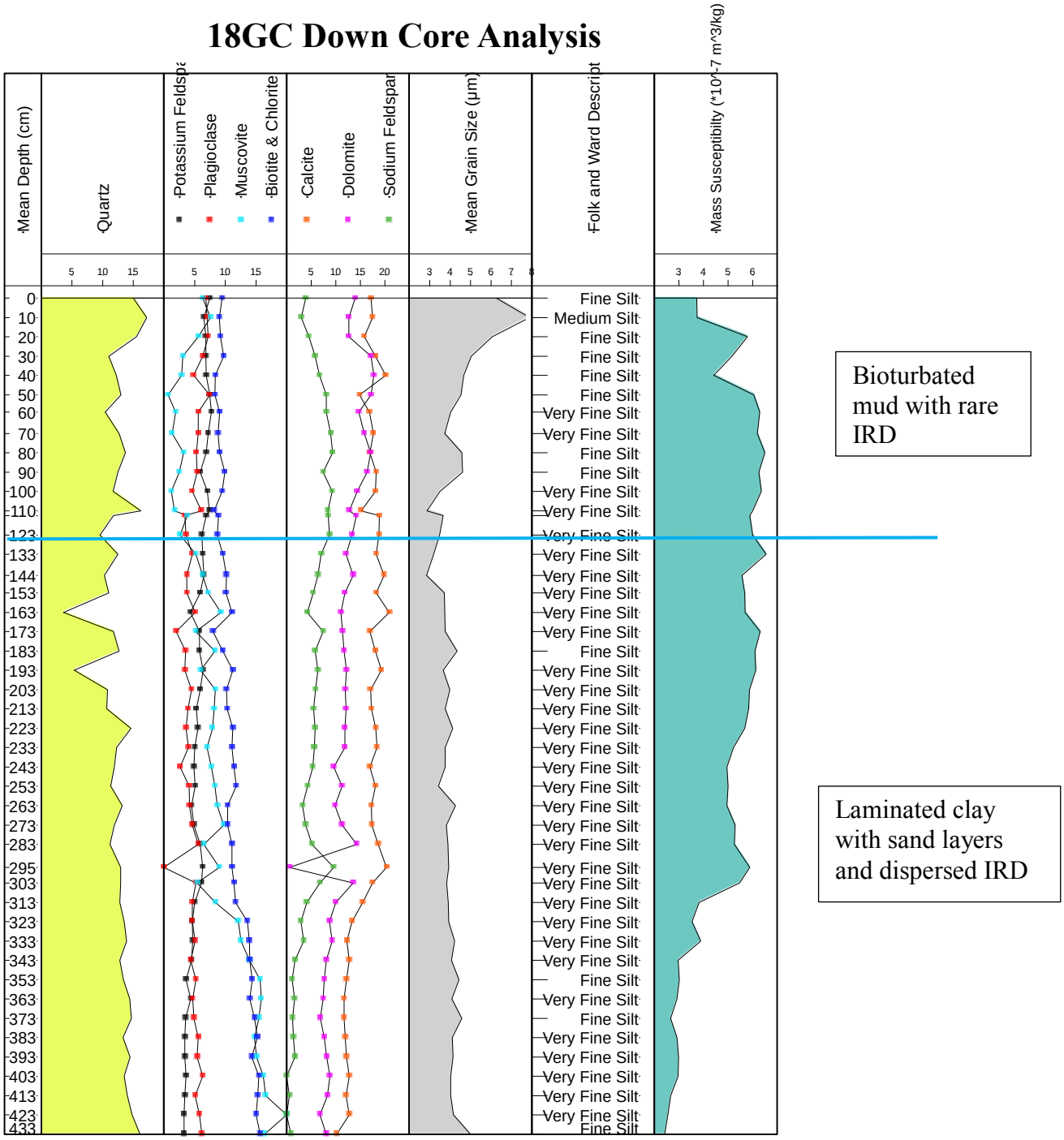

Figure 8b. Down core plot of 18GC graphically showing the measurements (taken using procedures in the Methods section of the theses) with depth. Weight percentages were accumulated from the RockJock v6 program (Eberl, 2003). Folk and Ward descriptors and mean grain size calculated by the GradiStat program (Blott and Pye, 2001).

DISCUSSION

Collaborative analysis of the three proxies explored for this thesis and the foraminiferal and radiocarbon dates are needed in order to produce a glacial history of the Petermann Glacier. Multiproxy analysis of the HLY03-05GC showed that the retreat of the Greenland Ice Sheet from Hall Basin had begun by 10,300 years BP, the age of the base of HLY03-05GC (Jennings et al., 2011) (Appendix A and *Figure 1*). Additional radiocarbon samples have been picked by other students, including myself, and researchers under the direction of Anne Jennings at INSTAAR to be analyzed to obtain their ^{14}C ages (Jennings et al., 2015). Unfortunately, some of the results from these samples have not been reported. Because of this, a relative deglaciation history of the Petermann Glacier will be proposed using the data available from the two cores of this study and the HLY03-05 GC data.

Based on their geographic locations, I suggest that 18GC would be first exposed to the entrainment of silt and clay particles in open water, as well to the introduction of IRD via icebergs due to its proximity to Kennedy Channel of Nares Strait. As the Greenland Ice Sheet was retreating 10,300 years ago, Hall Basin would receive glacial marine sediments. The opening of Nares Strait might be recorded by the shift to the upper lithofacies as seen in HLY03-05GC. The opening would allow currents to pass through entraining silt sized sediment within the currents and depositing them on the sea floor beginning at approximately 9,200 years ago (Jennings et al., 2011). As examined within the Results sections, 18GC is primarily composed of the laminated clay unit with mean grain sizes of fine to very fine silt, 3-7 microns in diameter (*Figure 8b)*. Based on the minimal variation within the grain size, mineralogy, and magnetic susceptibility with depth in 18GC, I propose that this core penetrated into the oldest sediments of the study but not into till. Its laminated clay unit is similar to that in the HLY03-05GC core and

many of the other cores collected in Hall Basin. The low numbers, but broadly dispersed coarse IRD in 18GC supports this hypothesis, as it indicates that ice rafting was rare but happening through the entirety of this core (*Figures 4, 8b*). The strong similarity between the mean grain size of the upper unit in the composite core and the laminated clay in 18GC suggests that they have similar depositional environments.

The basal units of the composite core, 003TC/41GC/003PC are coarser grained than any of the other units in the study. The presence of coarse IRD suggests that there were abundant icebergs, or in the case of the diamicton, possibly debris flow activity. The interesting shift to much finer mean grain size and the disappearance of IRD in the upper part of the composite core may reflect advance of the ice tongue over the outer fjord site. The ice tongue would protect this locality from iceberg ice rafting from the Petermann Glacier. By examining *Figure 8a* and the analysis discussed in the results section of the variation with depth, I propose that the coarse units below 465 cm represent an interval of entrainment and IRD introduction where the outer fjord was exposed to the grounding line of the Petermann Glacier and the ice shelf was not covering the site.

CONCLUSIONS

While this objective of this thesis was to provide a Late Quaternary Provenance glacial history of the Petermann Glacier and Hall Basin, lack of more sufficient ^{14}C dates only allow a relative glacial history to be proposed. The onset of the retreat of the Greenland and Innuitian Ice Sheets in Nares Strait began approximately 10,300 years BP (Jennings et al., 2011). With the retreat of the ice sheets came the opening of Hall Basin and deposition of glacial marine mud with almost no IRD. The strong comparison of the laminated clay to the upper unit in the fjord suggests that these might be at least in part sub ice shelf sediments. The opening of Nares Strait

and beginning of the through-flow of Arctic Ocean water to Baffin Bay may be reflected by the transition to the upper coarser unit in 18GC.

In the fjord the presence of coarser sediments indicates that during the early part of the record the outer fjord was exposed to the grounding line of the Petermann Glacier and not covered by the ice tongue. Additional radiocarbon dates are a high priority for further conclusions to be drawn.

While this thesis only provides a relative glacial history of Hall Basin and the Petermann Glacier, it provided critical mineralogical, grain size and magnetic susceptibility data to further examine this area along the Nares Strait. Further analysis of this data will undoubtedly be performed alongside the ongoing foraminifer analysis and other observations to compose a more complete Late Quaternary glacial history of Hall Basin and the Petermann Glacier.

ACKNOWLEDGEMENTS

The thesis was supported by funds from the National Science Foundation, Grant PLR-ANS1417784, A Collaborative Research: Petermann Glescher, Greenland Paleooceanography and Paleoclimatology to Drs Anne E. Jennings and John T. Andrews. The collaboration of data for this project and expedition was between researchers at INSTAAR- University of Colorado, Boulder, Stockholm University and CEOAS- Oregon State University. The many crewmembers and researchers aboard the *Oden* collected the cores, initial data, and logs during the expedition. The INSTAAR Sedimentology Lab Coordinator Wendy Roth provided instructions on the various techniques throughout the data collection process. John Andrews and Anne Jennings provided background material and comments on various drafts of the thesis. All of the committee members' dedication of their time, comments and advising throughout this process is greatly appreciated.

REFERENCES

Aitchison, J., 1992, On criteria for measures of compositional difference: Mathemtical Geology, v. 24, p. 365-379.

Aitchison, J., 1997, The one-hour course in compositional data analysis or compositional data analysis is simple, *in* Proceedings Proceedings International Association of Mathematical Geologists, Barcelona, 1997, p. 3-35.

Aitchison, J., 1999, Logratios and natural laws in compositional data analysis: Mathematical Geology, v. 31, no. 5, p. 563-579.

Blott, S. J., and Pye, K., 2001, GRADISTAT: A grain size distribution and statistics package for the analysis of unconsolidated sediments: Earth Surface Processes and Landforms, v. 26, no. 11, p. 1237-1248.

Davis, J. C., 1973, Statistics and Data Analysis in geology, New York, John Wiley & Sons, Inc., 550 pp.

Dyke, A. S., Andrews, J. T., Clark, P. U., England, J. H., Miller, G. H., Shaw, J., and Veillette, J. J., 2002: The Laurentide and Innuitian ice sheets during the Last Glacial Maximum. *Quaternary Science Reviews,* 21: 9-31.

Eberl, D. D., 2003, User guide to RockJock: A program for determining quantitative mineralogy from X-ray diffraction data: United States Geological Survey, Open File Report 03-78, 40 pp, 03-78, 45 pp.

England, J., 1974, Advance of the Greenland Ice Sheet on to north-eastern Ellesmere Island: Nature, v. 252, no. 5482, p. 373-375.

England, J., 1985. The late quaternary history of hall land, northwest Greenland. Can. J. Earth Sci. 22, 1394–1408.

England, J., 1999. Coalescent Greenland and Innuitian ice during the Last Glacial Maximum: revising the Quaternary of the Canadian High Arctic. *Quaternary Science Reviews,* 18: 421-456.

Geologic Survey of Denmark and Greenland. Geologic Map of Greenland [map]. 1:2500000. Copenhagen: GUES, 2003.

Ghosh, S., and Dubey, S. K., 2013, Comparitive analysis of K-means and Fuzzy C-means algorithms: International Journal of Advanced Computer Science and Technology, v. 4, p. 35-39.

Gigawiz Ltd. Co. *Aabel*. Computer software. Vers. 3. Gigawiz Ltd. Co., 2008. Web.

Jennings, A.E., Bailey, E., Oliver, B., Andrews, J.T., Prins, M., Troelstra, S., Stoner, J., Reilly, B., Daview-Walczak, M., Mix,Dec, 2015. Retreat of the coalescent Greenland and Innuitian ice sheets from Nares Strait. AGU Fall Meeting. PP51C-Feedbacks on Ice-Sheet Growth and Decay during the Last Glacial Cycle 1-Posters A. PP51C-2305.

Jennings, A. E., Sheldon, C., Cronin, T. M., Francus, P., Stoner, J., and Andrews, J., 2011, THE HOLOCENE HISTORY OF NARES STRAIT: Transition from Glacial Bay to Arctic-Atlantic Throughflow: Oceanography, v. 24, no. 3, p. 26-41.

KaleidaGraph. Computer software. Vers. 4.5.2. Synergy Software, 24 Apr. 2014. Web

Klein, Anna, "Lateral Variations in Sediment Provenance and Grain Size along the Baffin Island Slope" (2016). Undergraduate Honors Theses. 1107. http://scholar.colorado.edu/honr_theses/1107

Münchow, A., L. Padman, P. Washam, and K.W. Nicholls. 2016. The ice shelf of Petermann Gletscher, North Greenland, and its connection to the Arctic and Atlantic Oceans. Oceanography 29(4):xx–xx, https://doi.org/10.5670/oceanog.2016.xx.

Nick, F.M., A. Luckman, A. Vieli, C.J. Van Der Veen, D. Van As, R.S.W. Van De Wal, F. Pattyn, A.L. Hubbard, and D. Floricioiu. 2012. The response of Petermann Glacier, Greenland, to large calving events, and its future stability in the context of atmospheric and oceanic warming. Journal of Glaciology 58 (208):229–239, https://doi.org/10.3189/2012JoG11J242.

Schlitzer, R., Ocean Data View, https://odv.awi.de, 2016.

Thompson, R., Battarbee, R. W., O'Sullivan, P. E., and Oldfield, F., 1975, Magnetic susceptibility of lake sediments: Limnology & Oceanography, v. 20, no. 5, p. 687-698.

Thompson, R., Bloemendal, J., Dearing, J. A., Oldfield, F., Rummery, T. A., Stober, J. C., and Turner, G. M., 1980, Environmental Applications of Magnetic Measurements: Science, v. 207, p. 481-486.

Tinto, K.J., Bell, R.E., Cochran, J.R., Munchow, A., 2015. Bathymetry in Petermann fjord from Operation IceBridge aerogravity. *Earth and Planetary Science Letters*, 422: 58-66.

Walden, J., Smith, J. P., and Dackombe, R. V., 1992, Mineral magnetic analyses as a means of lithostratigraphic correlation and provenance indication of glacial diamicts: intra- and inter-unit variations: Journal of Quaternary Science, v. 7, p. 257-270.

APPENDIX

APPENDIX A.

Latitude and longitude coordinates of all the cores collected aboard the *Oden*, July-September 2015.

Station	Lon (°E)	Lat (°N)
003PC	-62.0682	81.1901
31PC	-64.35223333	81.61063333
33GC	-63.851	81.535
003UI	-60.7845	80.7373
04GC	-61.2534	80.9705
08GC	-61.7955	81.0947
12GC	-61.5452	80.9503
16GC	-62.54435	81.73327167
17GC	-62.17015	81.68413333
18GC	-62.2991	81.62646667
19GC	-62.3198	81.54935
25GC	-63.62999	81.28372
30GC	-64.3523	81.619775
43PC	-63.25466667	81.43376667
48PC	-64.317	81.30466667
49GC	-64.7655	81.13683333
18GC	-62.2991	81.62646667
003PC	-62.0682	81.1901
003TC	-62.0682	81.1901
31PC	-64.35223333	81.61063333
41GC	-61.97715	81.19378333

APPENDIX B. Core descriptions noting sediment properties, structures and any observable variation with depth. Core logs were recorded by Anne Jennings and other crewmembers on board the *Oden* icebreaker.

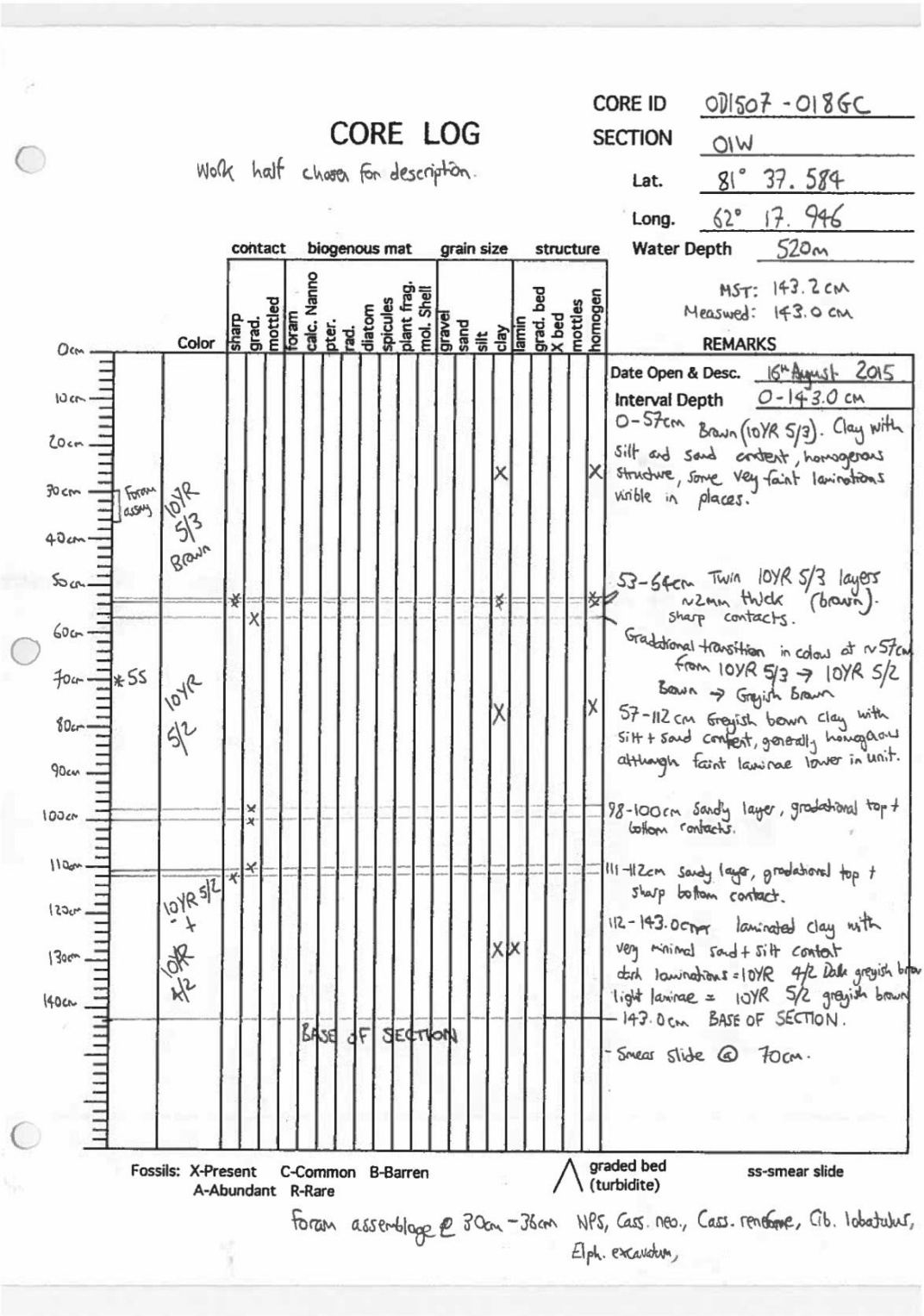

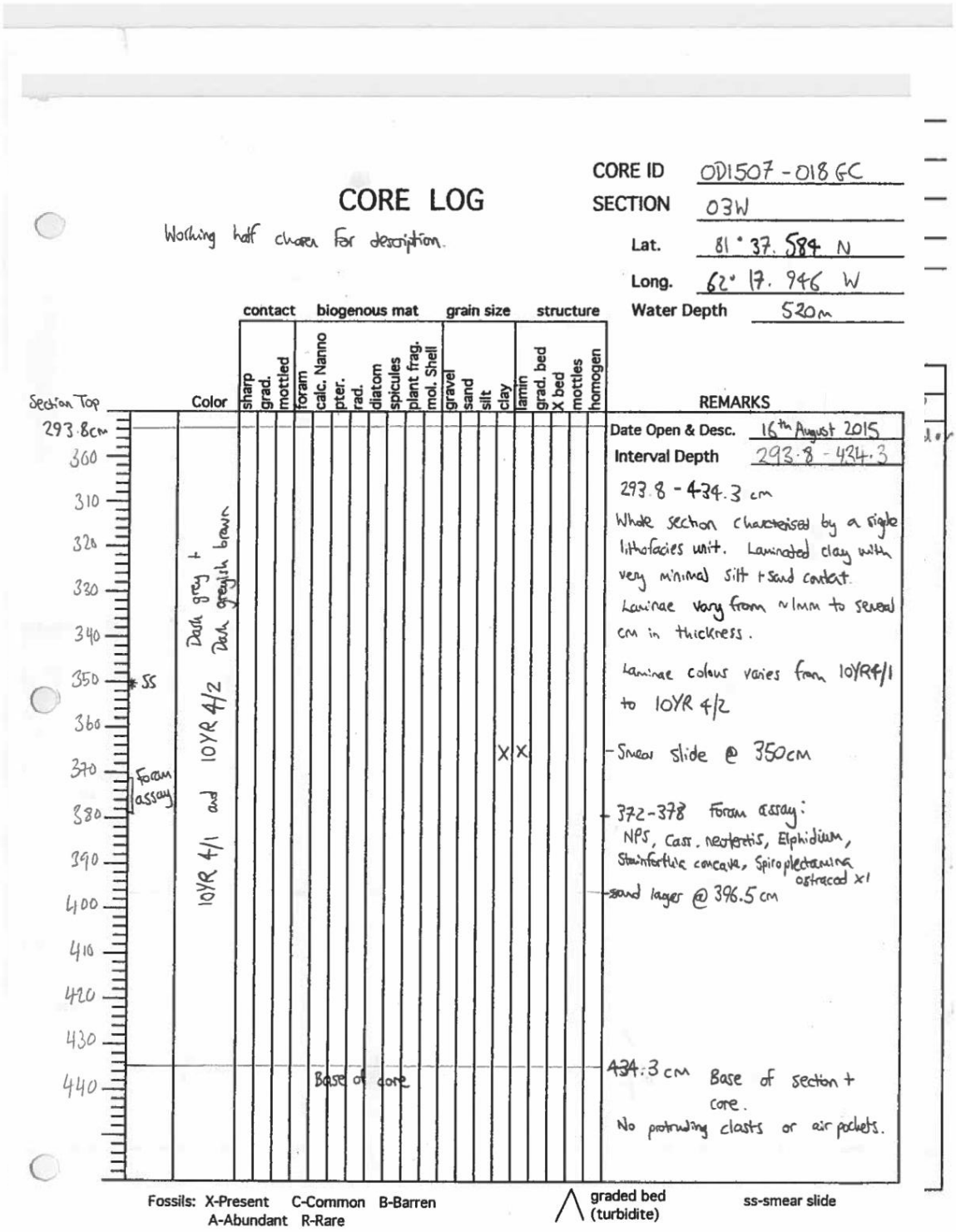
CORE LOG
Working half chosen for description.
CORE ID OD1507-018GC
SECTION 03W
Lat. 81° 37. 584 N
Long. 62° 17. 946 W
Water Depth 520m
contact
biogenous mat
grain size
structure
sharp
grad.
mottled
foram
calc. Nanno
pter.
rad.
diatom
spicules
plant frag.
mol. Shell
gravel
sand
silt
clay
lamin
grad. bed
X bed
mottles
homogen
Section Top
Color
REMARKS
293.8cm
360
310
320
330
340
350
360
370
380
390
400
410
420
430
440
SS
Foram assay
Dark grey + Dark greyish brown
10YR 4/1 and 10YR 4/2
X X
Date Open & Desc. 16th August 2015
Interval Depth 293.8 - 434.3
293.8 - 434.3 cm
Whole section characterised by a single lithofacies unit. Laminated clay with very minimal silt + sand content.
Laminae vary from ~1mm to several cm in thickness.
Laminae colours varies from 10YR4/1 to 10YR 4/2
- Smear slide @ 350cm
372-378 Foram assay:
NPS, Cass. neoteretis, Elphidium, Stainforthia concava, Spiroplectammina ostracod x1
- sand layer @ 396.5 cm
434.3 cm Base of section + core.
No protruding clasts or air pockets.
Base of core
Fossils: X-Present C-Common B-Barren
A-Abundant R-Rare
graded bed (turbidite)
ss-smear slide

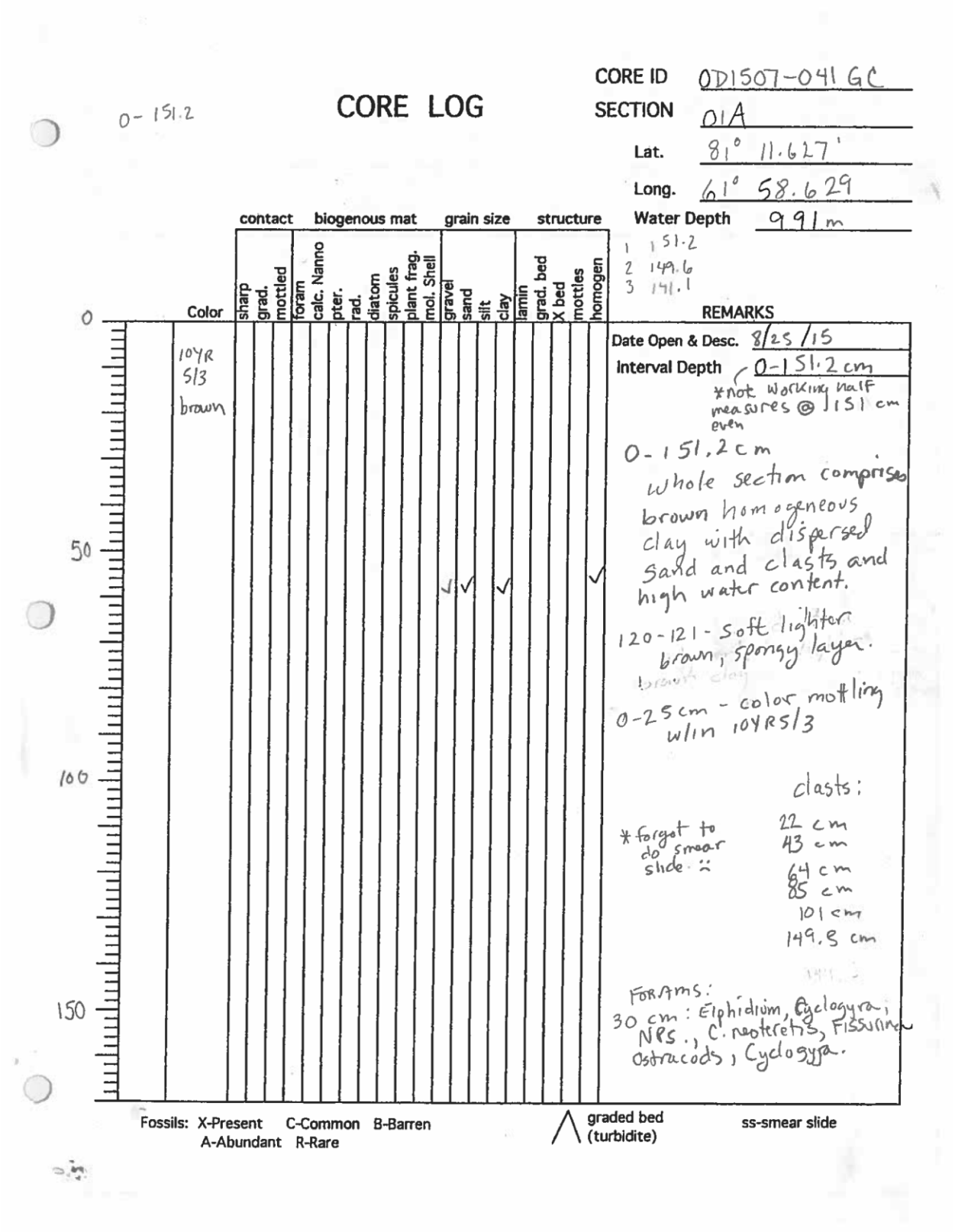

CORE LOG

0-151.2

CORE ID OD1507-041 GC
SECTION 01A
Lat. 81° 11.627'
Long. 61° 58.629
Water Depth 991 m

1 151.2
2 149.6
3 141.1

contact: sharp, grad., mottled
biogenous mat: foram, calc. Nanno, pter., rad., diatom, spicules, plant frag., mol. Shell
grain size: gravel, sand, silt, clay
structure: lamin, grad. bed, X bed, mottles, homogen

Color: 10YR 5/3 brown

0
50
100
150

REMARKS

Date Open & Desc. 8/25/15
Interval Depth 0-151.2 cm
*not working half measures @ 151 cm even

0-151.2 cm
whole section comprises brown homogeneous clay with dispersed sand and clasts and high water content.

120-121 - soft lighter brown, spongy layer.

0-25 cm - color mottling w/in 10YR5/3

clasts:
22 cm
43 cm
64 cm
85 cm
101 cm
149.8 cm

*forgot to do smear slide :(

FORAMS:
30 cm: Elphidium, Cyclogyra, NPS., C. neoteretis, Fissurina, Ostracods, Cyclogyra.

Fossils: X-Present C-Common B-Barren
A-Abundant R-Rare

graded bed (turbidite)

ss-smear slide

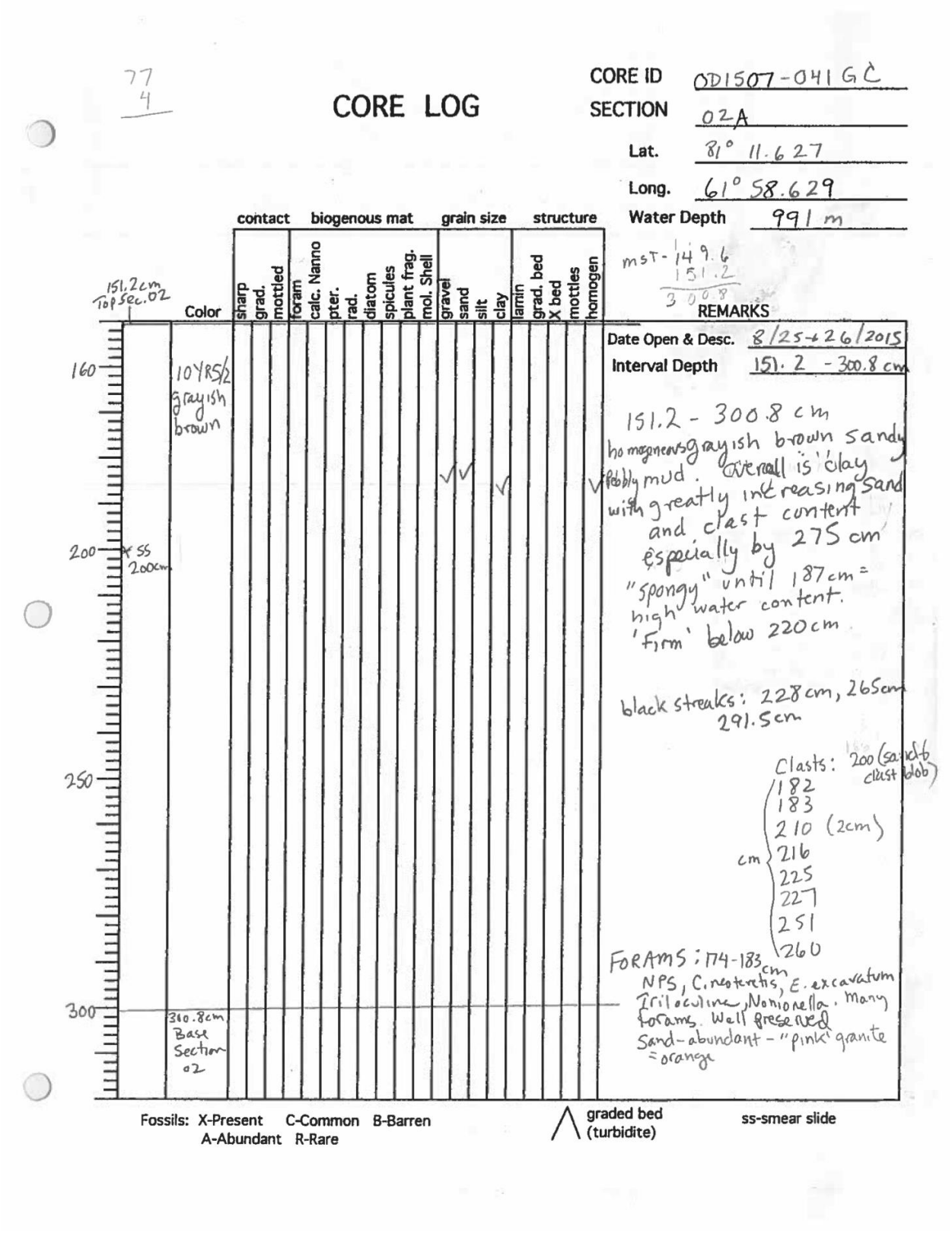
77
4
CORE LOG
CORE ID OD1507-041GC
SECTION 02A
Lat. 81° 11.627
Long. 61° 58.629
Water Depth 991 m
MST - 149.6
151.2
300.8
contact
biogenous mat
grain size
structure
sharp
grad.
mottled
foram
calc. Nanno
pter.
rad.
diatom
spicules
plant frag.
mol. Shell
gravel
sand
silt
clay
lamin
grad. bed
X bed
mottles
homogen
151.2cm Top Sec. 02
Color
REMARKS
Date Open & Desc. 8/25-26/2015
Interval Depth 151.2 - 300.8 cm
160
200
250
300
10YR5/2 grayish brown
SS 200cm
151.2 - 300.8 cm homogeneous grayish brown sandy pebbly mud. Overall is clay with greatly increasing sand and clast content especially by 275 cm "spongy" until 187cm = high water content. 'Firm' below 220cm
black streaks: 228cm, 265cm 291.5cm
Clasts: 200 (sand to clast blob)
cm
182
183
210 (2cm)
216
225
227
251
260
FORAMS: 174-183 cm
NPS, C. neoteretis, E. excavatum
Triloculina, Nonionella. Many forams. Well preserved
Sand-abundant - "pink" granite = orange
310.8cm Base Section 02
Fossils: X-Present C-Common B-Barren
A-Abundant R-Rare
graded bed (turbidite)
ss-smear slide

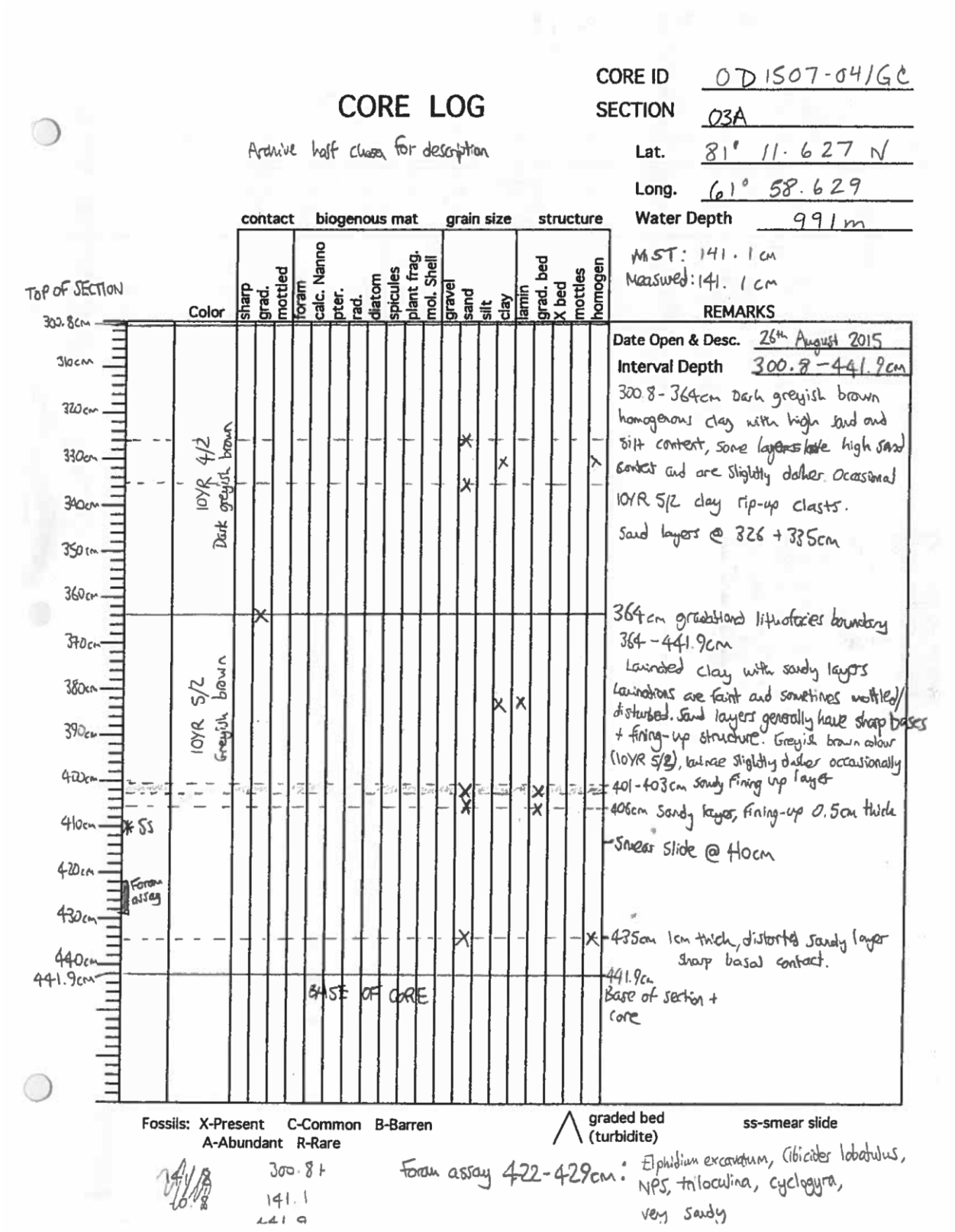
CORE LOG
Archive half closed for description
CORE ID OD1507-04/GC
SECTION 03A
Lat. 81° 11.627 N
Long. 61° 58.629
Water Depth 991m
MST: 141.1cm
Measured: 141.1cm
TOP OF SECTION
contact
biogenous mat
grain size
structure
Color
sharp
grad.
mottled
foram
calc. Nanno
pter.
rad.
diatom
spicules
plant frag.
mol. Shell
gravel
sand
silt
clay
lamin
grad. bed
X bed
mottles
homogen
REMARKS
10YR 4/2 Dark greyish brown
10YR 5/2 Greyish brown
Foram assay
SS
BASE OF CORE
Date Open & Desc. 26th August 2015
Interval Depth 300.8-441.9cm
300.8-364cm Dark greyish brown homogenous clay with high sand and silt content, some layers have high sand content and are slightly darker. Occasional 10YR 5/2 clay rip-up clasts.
Sand layers @ 326 + 335cm
364cm gradational lithofacies boundary
364-441.9cm
Laminated clay with sandy layers
Laminations are faint and sometimes mottled/disturbed. Sand layers generally have sharp bases + fining-up structure. Greyish brown colour (10YR 5/2), laminae slightly darker occasionally
401-403cm sandy fining up layer
406cm Sandy layer, fining-up 0.5cm thick
Smear slide @ 410cm
435cm 1cm thick, distorted sandy layer
Sharp basal contact.
441.9cm
Base of section + core
Fossils: X-Present C-Common B-Barren
A-Abundant R-Rare
graded bed (turbidite)
ss-smear slide
300.8
141.1
441.9
Foram assay 422-429cm: Elphidium excavatum, Cibicides lobatulus, NPS, triloculina, cyclogyra, very sandy

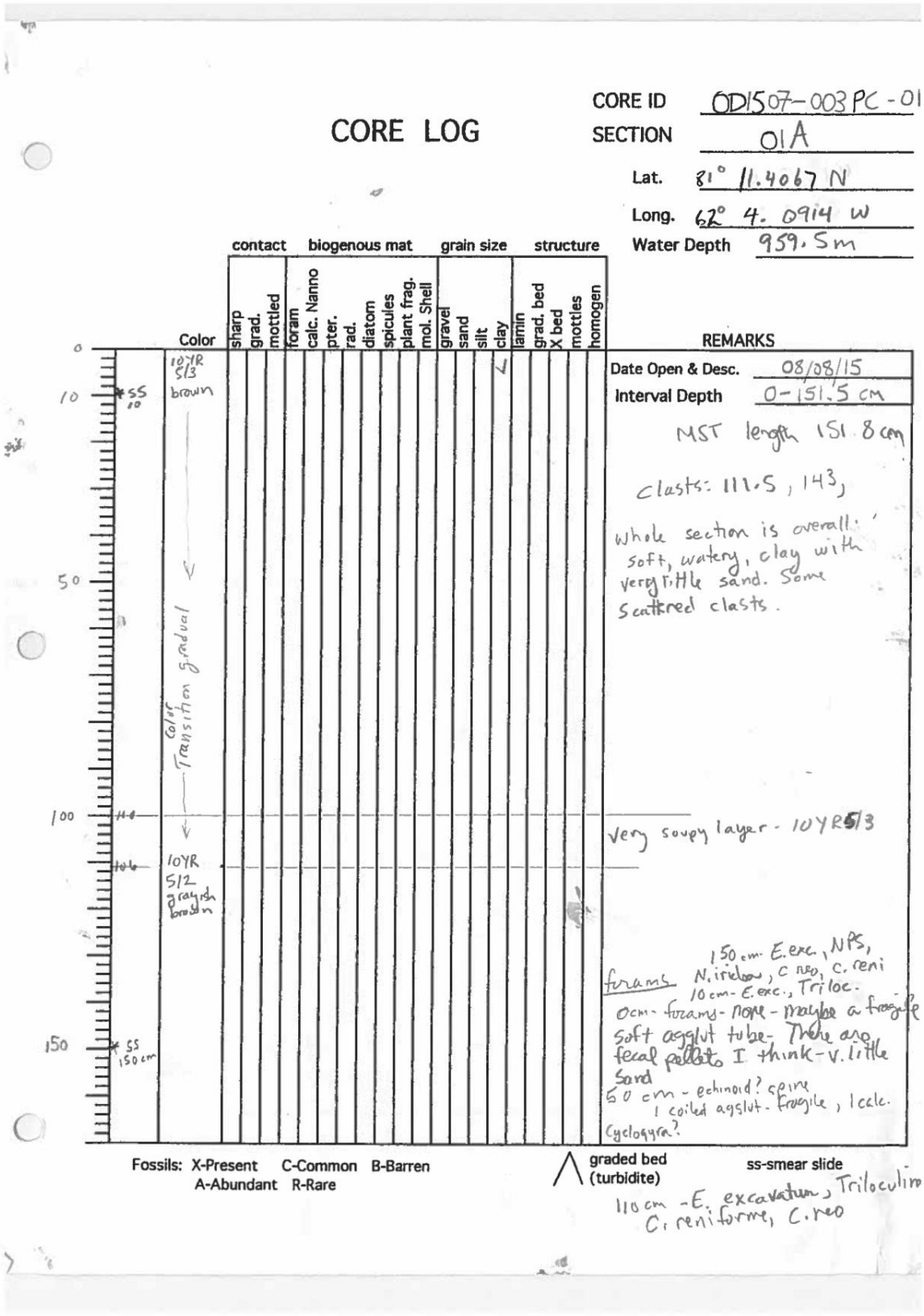
CORE LOG
CORE ID OD1507-003PC-01
SECTION 01A
Lat. 81° 11.4067 N
Long. 62° 4.0914 W
Water Depth 959.5m
contact
biogenous mat
grain size
structure
sharp
grad.
mottled
foram
calc. Nanno
pter.
rad.
diatom
spicules
plant frag.
mol. Shell
gravel
sand
silt
clay
lamin
grad. bed
X bed
mottles
homogen
Color
REMARKS
Date Open & Desc. 08/08/15
Interval Depth 0-151.5 cm
MST length 151.8 cm
Clasts: 111.5, 143,
Whole section is overall soft, watery, clay with very little sand. Some scattered clasts.
Color Transition gradual
very soupy layer - 10YR 5/3
10YR 5/2 grayish brown
150 cm E.exc, NPS, N.iridea, C reo, C. reni
10 cm - E.exc., Triloc.
0 cm - forams - none - maybe a fragile soft agglut tube. There are fecal pellets I think - v. little sand
50 cm - echinoid? spine
1 coiled agglut - fragile, Icele. Cyclogyra?
110 cm - E. excavatum, Triloculina C. reniforme, C. reo
Fossils: X-Present C-Common B-Barren
A-Abundant R-Rare
graded bed (turbidite)
ss-smear slide

CORE LOG

CORE ID OD1507-003PC-
SECTION 03 W
Lat. 81° 11.4067N
Long. 62° 4.0914 W
Water Depth 959.5 m

301.5
150.2
451.7

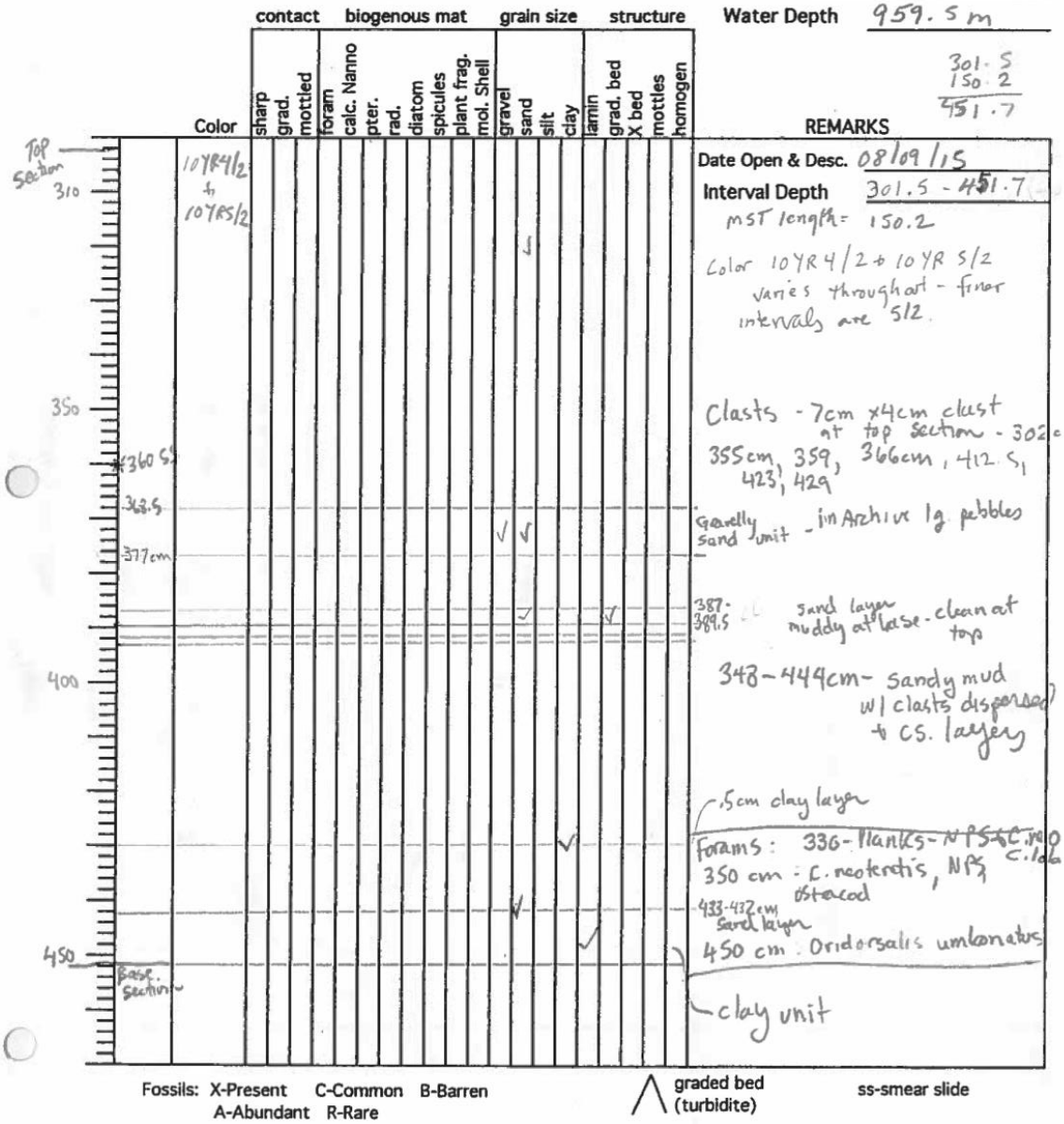

Fossils: X-Present C-Common B-Barren
A-Abundant R-Rare

graded bed (turbidite)

ss-smear slide

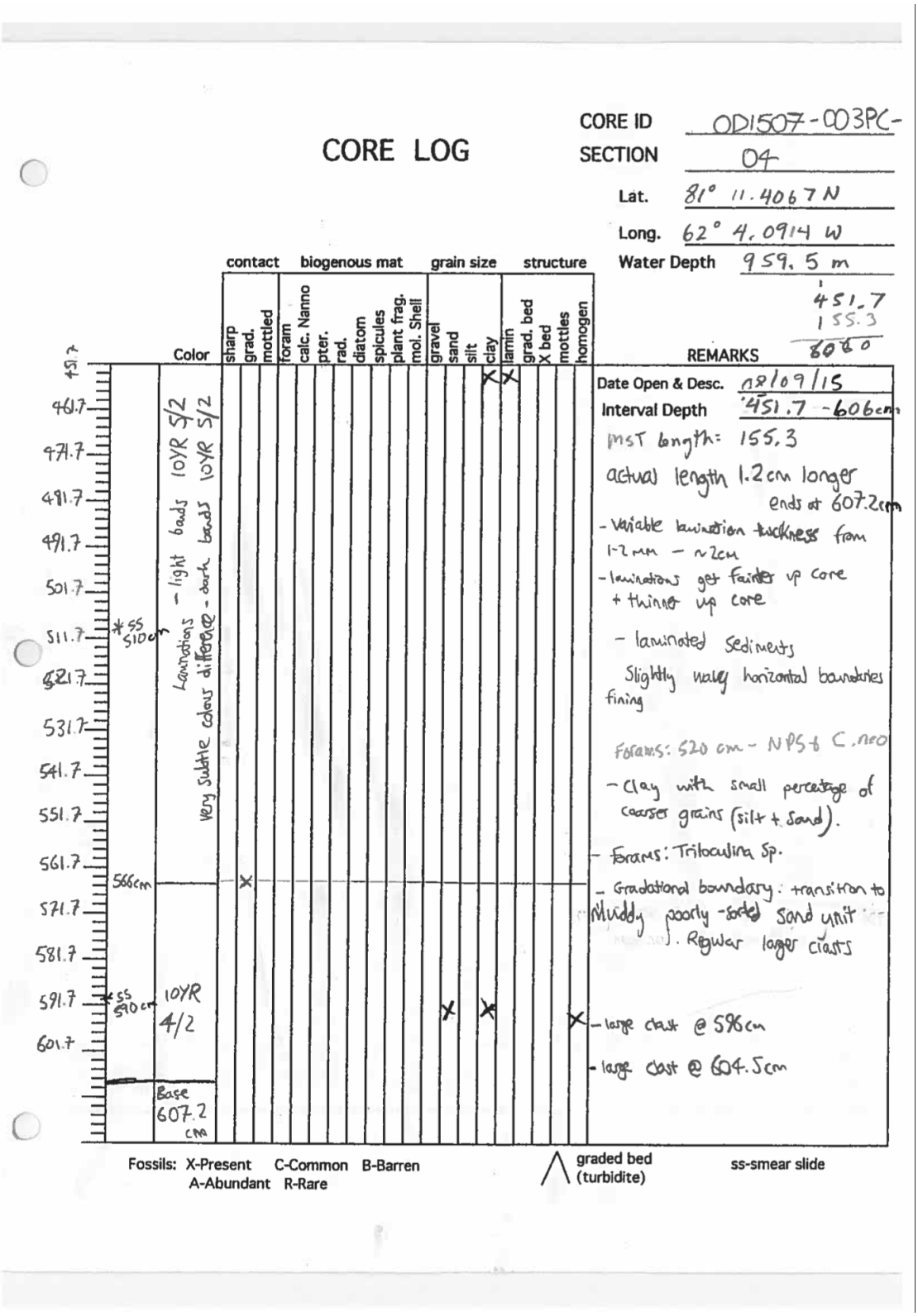
CORE LOG
CORE ID ODI507-003PC-
SECTION 04
Lat. 81° 11.4067 N
Long. 62° 4.0914 W
Water Depth 959.5 m
451.7
155.3
606.0
contact
biogenous mat
grain size
structure
sharp
grad.
mottled
foram
calc. Nanno
pter.
rad.
diatom
spicules
plant frag.
mol. Shell
gravel
sand
silt
clay
lamin
grad. bed
X bed
mottles
homogen
Color
REMARKS
Date Open & Desc. 18/09/15
Interval Depth 451.7 -606cm
mST length: 155.3
actual length 1.2cm longer
ends at 607.2cm
- variable lamination thickness from 1-2 mm – ~2cm
- laminations get fainter up core + thinner up core
- laminated sediments
Slightly wavy horizontal boundaries fining
Forams: 520 cm - NPS & C. neo
- clay with small percentage of coarser grains (silt + sand).
- Forams: Triloculina Sp.
- Gradational boundary: transition to muddy poorly-sorted sand unit. Rogwar larger clasts
- large clast @ 596cm
- large clast @ 604.5cm
461.7
471.7
481.7
491.7
501.7
511.7
521.7
531.7
541.7
551.7
561.7
571.7
581.7
591.7
601.7
*SS 510cm
Laminations - light bands 10YR 5/2
dark bands 10YR 5/2
very subtle colour difference
566cm
*SS 590cm
10YR 4/2
Base 607.2 cm
Fossils: X-Present A-Abundant C-Common R-Rare B-Barren
graded bed (turbidite)
ss-smear slide

APPENDIX C.

Conversion of the raw Total Susceptibility to Mass Susceptibility calculated for the given depths of the 003TC/41GC/003PC composite core and 18GC cores. Results for Mass Susceptibility are listed in 10^{-7} m^3/kg.

	GRL	Mean Depth (cm)	Weight (grams)	Averaged Total Susceptibility Output (m^3)	Mass Susceptibility (m^3 /kg)
003TC	26405	8	6.65	36.5	5.48872E-07
	26406	20	8.01	36	4.49438E-07
	26407	25	8.46	34	4.01891E-07
	26408	29	6.91	33.5	4.84805E-07
	26409	35	7.56	39.5	5.22487E-07
	26410	41	7.5	40	5.33333E-07
	26411	49	8.18	38	4.64548E-07
41GC	26439	53.72	8.17	42.5	5.20196E-07
	26440	63.72	6.97	41.5	5.95409E-07
	26441	73.72	6.38	37	5.79937E-07
	26442	83.72	7.85	43	5.47771E-07
	26443	93.72	7.07	35.5	5.02122E-07
	26444	103.72	7.65	37	4.8366E-07
	26445	113.72	7.76	34	4.38144E-07
	26446	123.72	7.64	30.5	3.99215E-07
	26447	133.72	7.8	33.5	4.29487E-07
	26448	143.72	6.93	29.5	4.25685E-07
	26449	153.72	6.9	34.5	0.0000005
	26450	163.72	8.42	30	3.56295E-07
	26451	173.72	7.87	24	3.04956E-07
	26452	183.72	7.44	23	3.0914E-07
	26453	193.72	7.93	19	2.39596E-07
	26454	203.72	7.55	24.5	3.24503E-07
	26455	213.72	7.86	22.5	2.8626E-07
	26456	223.72	7.05	19.5	2.76596E-07
	26457	233.72	7.82	22.5	2.87724E-07
	26458	243.72	7.96	31	3.89447E-07
	26459	253.72	7.45	31.5	4.22819E-07
	26460	263.72	8.52	32	3.75587E-07
	26461	273.72	8.44	44	5.21327E-07
	26462	283.72	8.57	49	5.71762E-07
	26463	293.72	7.88	49	6.21827E-07
	26464	303.72	8.29	46	5.54885E-07
	26465	313.72	8	53.5	6.6875E-07
	26466	323.72	8.37	65.5	7.82557E-07
	26467	333.72	8.81	68	7.7185E-07
	26468	343.72	7.48	64	8.55615E-07
	26469	353.72	9.57	52.5	5.48589E-07
	26470	363.72	10.1	122	1.20792E-06
	26471	373.72	8.23	74	8.99149E-07
	26472	383.72	10.45	108	1.03349E-06
	26473	393.72	10.34	66	6.38298E-07

	26474	403.72	9.02	35.5	3.9357E-07
003PC	26390	414.62	7.7	58.5	7.5974E-07
	26391	424.62	8.49	55	6.47821E-07
	26392	434.62	9.33	56.5	6.05573E-07
	26393	444.62	9.26	58	6.2635E-07
	26394	454.62	8.84	47	5.31674E-07
	26395	464.62	9.84	46.5	4.72561E-07
	26396	474.62	9.43	50	5.30223E-07
	26397	484.62	9.2	40.5	4.40217E-07
	26398	494.62	9.16	35.5	3.87555E-07
	26399	504.62	10.69	34.5	3.22732E-07
	26400	514.62	10.67	67.5	6.32615E-07
	26401	524.62	6.81	79.5	1.1674E-06
	26402	534.62	10.31	186	1.80407E-06
	26403	544.62	13.74	147.5	1.07351E-06
	26404	554.62	7.36	83	1.12772E-06

Core	**GRL**	**Mean Depth (cm)**	**Weight (grams)**	**Averaged Total Susceptibility Output (m^3)**	**Mass Susceptibility** (m^3 /kg)
18GC	26475	0.5	7.39	27.5	3.72124E-07
	26476	10.5	8.95	33.5	3.74302E-07
	26477	20.5	7.69	44.5	5.78674E-07
	26478	30.5	7.94	41	5.16373E-07
	26479	40.5	6.23	27.5	4.41413E-07
	26480	50.5	7.45	45	6.04027E-07
	26481	59.5	6.91	43.5	6.29522E-07
	26482	70.5	7.11	44	6.18847E-07
	26483	80.5	7.23	47	6.50069E-07
	26484	90.5	8.54	53.5	6.26464E-07
	26485	100.5	8.18	52	6.35697E-07
	26486	110.5	3.58	21.5	6.00559E-07
	26487	113	7.39	43.5	5.88633E-07
	26488	123	7.84	47	5.9949E-07
	26489	133	8.7	57	6.55172E-07
	26490	144	8.45	47	5.56213E-07
	26491	153	8.45	48	5.68047E-07
	26492	163	8.79	50	5.68828E-07
	26493	173	8.72	55	6.30734E-07
	26494	183	7.38	45	6.09756E-07
	26495	193	7.27	44.5	6.12105E-07
	26496	203	7.92	46.5	5.87121E-07
	26497	213	7.97	46.5	5.83438E-07
	26498	223	9.07	51.5	5.67806E-07
	26499	233	8.22	43	5.23114E-07
	26500	243	6.86	34	4.95627E-07
	26501	253	8.61	43	4.99419E-07
	26502	263	8.39	41.5	4.94636E-07
	26503	273	7.19	38	5.28512E-07
	26504	283	8.46	44.5	5.26005E-07
	26505	295	7.64	45	5.89005E-07
	26506	303	8.77	48	5.4732E-07

26507	313	8.89	34	3.82452E-07
26508	323	8.08	28.5	3.52723E-07
26509	333	7.84	30.5	3.89031E-07
26510	343	8.62	25.5	2.95824E-07
26511	353	7.98	24	3.00752E-07
26512	363	7.74	22.5	2.90698E-07
26513	373	8.49	22.5	2.65018E-07
26514	383	7.2	21	2.91667E-07
26515	393	8.04	24	2.98507E-07
26516	403	8.42	25	2.96912E-07
26517	413	6.96	18.5	2.65805E-07
26518	423	6.9	17.5	2.53623E-07
26519	433	8.08	19.5	2.41337E-07

Thompson, R., Battarbee, R. W., O'Sullivan, P. E., and Oldfield, F., 1975, Magnetic susceptibility of lake sediments: Limnology & Oceanography, v. 20, no. 5, p. 687-698.

Walden, J., Smith, J. P., and Dackombe, R. V., 1992, Mineral magnetic analyses as a means of lithostratigraphic correlation and provenance indication of glacial diamicts: intra- and inter-unit variations: Journal of Quaternary Science, v. 7, p. 257-270.